TU Delft
Delft University of Technology

Erasmus MC
University Medical Center Rotterdam

Design and prototype of an electrode array for biventricular electrophysiological mapping

An 3D printed electrode array that minimally interferes with cardiac function

Master of Science Thesis

J.V. Buters

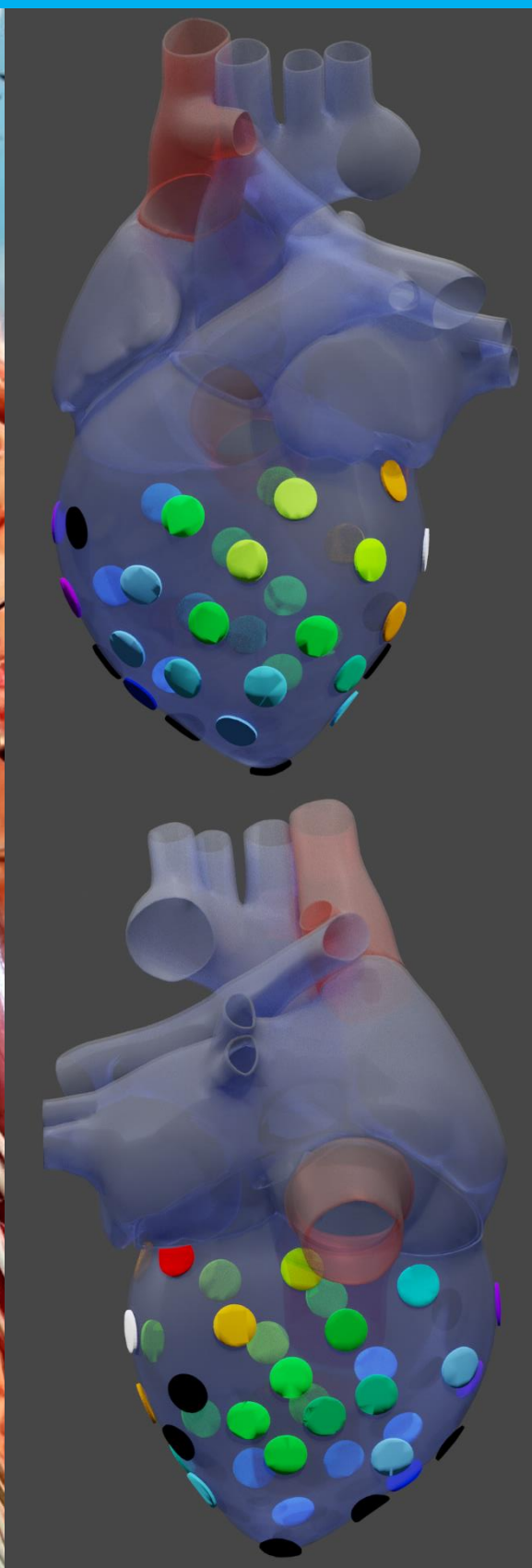

Design and prototype of an electrode array for biventricular electrophysiological mapping

An 3D printed electrode array that minimally interferes with cardiac function

By

Jeroen Victor Buters

to obtain the degree of Master of Science in Biomedical Engineering at the Delft University of Technology

Supervisor:	Prof. Dr. Ir. R. Dekker
	Prof. Dr. N.M.S. de Groot
	Dr. Y.J.H.J. Taverne
Daly supervisor:	Ir. J. H. Amesz
Thesis committee:	Prof. Dr. Ir. R. Dekker
	Prof. Dr. N.M.S. de Groot
	Dr. Y.J.H.J. Taverne
	Prof. Dr. P.J. French

Summary

Disturbances in the propagation of the electrical wavefront can cause cardiac arrhythmia's that can, in extreme cases, lead to cardiac arrest. By recording the electrical signals of the heart, a better understanding can be gained of the mechanisms behind cardiac arrhythmias. A method that can be used to investigate the state of the heart is electroanatomic mapping (EAM), where the local electrical activity is related to a point within a 3D anatomical reconstruction of the heart. By investigating the electrical activity, areas of scarring can be identified.
Currently, the electrical activity is recorded with a plaque multi-electrode array at the Erasmus MC. Local activation maps can be recorded during sinus rhythm (SR), and with the use of a reference electrode, total activation maps are generated. This can only be done during SR. During arrhythmia's, this is no longer possible due to temporal variation in electrical activity. To investigate the activation maps during arrhythmia, an electrode array that can record the total activity of the ventricles was designed and developed in this thesis.
By studying the literature and with the help of medical experts, a requirement list was established. Different concept ideas were compared using a Harris profile to select the best design for further development.
From the Harris profile it was concluded that a 3D printed sock was the best design for the electrode array. An investigation of the effects of the pattern and thickness on the stiffness and fatigue life of the sock were performed with the help of tensile tests and fatigue tests. From the results of the tensile and fatigue tests, a decision for the design of the electrode array was made. A 3D printed sock with the optimized design and electrodes were used to make epicardial recordings on a porcine heart in an ex vivo heart perfusion setup. The electrical recordings were later analyzed and visualized on a 3D model of the heart.
Even though the resolution of the electrode array was lower than that of the epicardial mappings performed at the Erasmus MC, the results obtained from the electrode array looked promising. This is the first study that has developed a 3D printed electrode array the can record the electrical activity of the ventricular surface from multiple sites simultaneously. However, before the electrode array can be used for elucidating the mysteries behind epicardial activation during arrhythmia's, further development is needed.

Acknowledgements

This study would not have been possible without the help of others. For this reason I would like to express my gratitude for their support and help during my thesis.
I would like to thank my supervisors Dr. Yannick Taverne and Prof. Dr. Natasja de Groot for, giving me the opportunity to work on this project, having me at the Erasmus MC, and guidance during my stay. I was able to learn a lot on cardiac electrophysiology and organ perfusion.

I would like to thank Prof. Ir. Ronald Dekker for his guidance and help during this project. Our discussions showed me new insights on how to tackle the challenges during my thesis. Furthermore, I am grateful for helping me connection me with experts that could help me with my thesis.

I want to thank Ir. Jorik Amezs for his daily guidance and constant help during my stay at the Erasmus MC. Working together with you was a real pleasure. Furthermore, I would like to thank all the colleagues at the department of “translationele elektrofysiologie” for giving me a warm welcome and the enjoyable discussions.

In addition, I would like to give a big thank you to Darragh Walsh and Fabien Bruning. Without their help and expertise it would not have been possible to have accomplished reach the current design. For letting me use the 3D printer day in and day out.

Finally, I would like to thank Sophie listening to my thoughts even though they were not always comprehensible, For supporting me throughout my thesis

Nomenclature

Abbreviations

3D	Three dimensional
ASIC	Application specific integrated circuit
DBD	Donation after brain death
DCD	Donation after circulatory death
E_a	Apparent Young's modulus
EAM	Electroanatomic mapping
EVHP	*ex vivo* heart perfusion
FOSS	Fiber optic shape sensing
LV	Left ventricle
O_2	Oxygen
UTS	Ultimate tensile strength
RV	Right ventricle
SR	Sinus rhythm
TAT	Total activation time

Contents

1. Introduction

The contractions of the heart follow the electrical wavefront that propagates across the myocardial wall. Under normal circumstances, electrical wavefronts travel in a regular pattern over the heart. Disturbances in the propagation of the electrical wavefront can cause cardiac arrhythmia's that can, in extreme cases, lead to cardiac arrest. By recording the electrical signals of the heart, a better understanding can be gained of the mechanisms behind cardiac arrhythmia's [2, 18].

1.1. Cardiac mapping

Electroanatomic mapping (EAM) records the electrical activation in relation to the anatomical location on the heart [5]. By measuring the electrical activity of the heart, activation patterns can be visualized with activation maps. From the activation maps, the direction of activation, areas of conduction delay and block can be derived [11]. This can be used to investigate abnormalities in the activation patterns. In general they are the result of; disorders of impulse formation, disorders of impulse conduction, or a combination of both [20].

EAM is utilized in the identification of arrhythmogenic substrate, where areas scarring are identified. These areas are associated with the pathways for re-entrant circuits which cause abnormal heart rhythms [11, 16]. In re-entrant circuits, the electrical signal persists and re-excites the heart after the after the initial activation wavefront [3, 17]. In areas where scar tissue has formed, the amplitude of the recorded electrical signals is reduced due to the structural changes in the tissue [11]. Identifying the amount of scar tissue of the heart can help to determine the state of the heart. However, successful detection of areas with low amplitude is still difficult. The cut-off amplitude of the electrical signals to distinguish between healthy and scar tissue has not yet been well-defined. Animal model experiments on *ex vivo* heart perfusion (EVHP) systems have been performed to determine the correct cut-off value for finding scar tissue in the heart. But, they have been unsuccessful, and it was difficult to extrapolate to humans [11, 16]. Substrate mapping on EVHP models can help to give insight on the state of the heart. Substrate mapping can also be used to shed more light on finding causes of arrhythmias, as it can identify areas that can cause conduction blockades [22].

Currently, at the Translational Electrophysiology Lab of the Erasmus Medical Center, epicardial mapping is performed with a high-density plaque electrode array with 192 electrodes (see figure 1). A plaque electrode was moved along imaginary lines between anatomical borders of the heart, and five second recordings of the local activation were made.. During regular heart rhythms, like sinus rhythm (SR), global activation times of the local activation maps were calculated with the help of a reference electrode. The local activation maps were used to reconstruct and visualize the electrical activity of the whole heart on a 3D model [30].

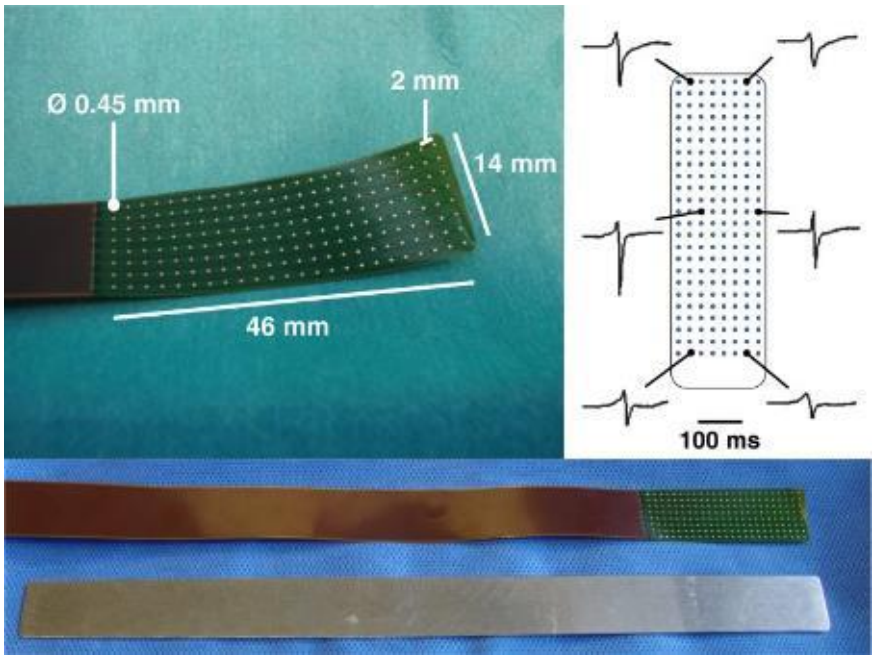

Figure 1. Plague electrode array used for high resolution mapping. Image taken from [30]

1.2. Problem definition

During arrhythmia, the heart beats with an irregular rhythm, and therefore it is not possible to visualize the global activation pattern of the heart. The electrical activity is disorganized and the activation patterns are different for each heartbeat. To analyze the total heart activity during arrhythmia, the electrical activity of the whole heart has to be recorded simultaneously. Therefore, a device that can record the electrical activity and the position of each recording electrode, without obstructing the heart function is needed. This will reduce the time needed for mapping, and total activation maps can be obtained during arrhythmia.

1.3. Study goal

The goal of this study is to design, fabricate and test a prototype of an electrode array that is able to simultaneously record the total activation patterns on the surface of the ventricles.

1.4. Study lay-out

The next chapter discusses the steps taken in designing the electrode array, the list of requirements, concept ideas, and selection for the optimal design. Finally, the design choices for the prototype are explained. In Chapter 3, the experimental setup for the material properties tests, fabrication of the electrode array, and the proof of concept are discussed. The results of the experimental tests and the proof of concept are summarized in Chapter 4. In Chapter 5 the test results and the prototype are discussed. Finally, in Chapter 6 the whole thesis is concluded.

2. Design process

The problem of designing the electrode array consists of three parts; 1. Designing the sock to cover the heart, 2. Mounting the electrode on the sock, and 3. Locating the electrode positions on the heart. In this study a sock was defined as a structure that can be put over an object. The next section the requirements for the electrode array are discussed, the different concept ideas are explained and compared in a Harris profile. In the final section the discusses the design step taken for the fabrication of the electrode array

2.1. Requirements

A list of requirements for the electrode array was created in collaboration with cardiac surgeons and electrophysiologist. The requirements list created in this study was a list of the ideal requirements for electrode array.

2.1.1. Heart impairment

The electrode array exerts a pressure on the epicardial tissue the heart. If the force the electrode array was to there is a risk of impairing the cardiac function. When the external pressure becomes higher than the internal pressure of the ventricles, they can collapse [6]. In the literature, it was found that normal right ventricle (RV) systolic pressure was 20–30 mmHg and normal diastolic pressure, 3–7 mmHg [19]. Therefore, to prevent the collapse of the RV the exerted pressure may not be higher than 20 mmHg or 2,7 kPa[19]. The pressure of the RV was chosen as the ventricular wall of the RV is thinner than the left ventricle (LV).

2.1.2. Good contact with the heart.

The goal of the electrode array was to record the electrical activation of the epicardium. To record an electrical signal, the electrodes had to make good contact with the epicardial surface. In the literature is was found that a force of 0.1 N was needed for electrodes to make proper contact for measuring electrical activity [11]. A force lower than 0.1 N causes noise in the data[11].Furthermore, the sock must have a good fit over the heart to facilitate the electrode contact with the epicardium.

2.1.3. Elastic

The heart is a muscle that is constantly contracting and changing shape. If the electrode array was rigid, the position of the electrodes on the heart would change during contraction and the electrode array would affect the function of the heart.

2.1.4. Ease of use

Currently, the time needed for EAM of the atria is approximately 10 min [30]. The device for recording the epicardial activity of the ventricles should have a similar procedure time. Furthermore, the electrode array must be handled with ease. As it will increase the operation time.

2.1.5. Transparency

The electrode array should be transparent. The surgeon had to be able to inspect the surface of the heart . A surgeon can tell a lot about the state of the heart when looking at the surface. If the view is obstructed, this information would be lost.

2.1.6. Sterilizability

To perform mapping studies on human hearts, the equipment has to be sterile. Sterilization could influence the properties of the electrode array, since the procedure can degrade the material. For this reason, the properties of the electrode array could not be different after sterilization.

2.1.7. High resolution

The mapping studies that have been done made use of a flexible electrode array that had an inter electrode distance of 2.5 mm [30]. To be able to compare the activation maps of the electrode array to the activation maps of current studies. The resolution of the electrode array should be equal to or higher than the 2.5mm.

2.1.8. Electrode localization

To interpret the results of the electrical signals, the location of the electrodes on the heart has to be known. Without the location of the recording site, it would be impossible to locate the source of arrhythmias.

2.2. Concept designs

With the design requirements in mind, several concept designs have been created with the focus on making contact with the heart. Finally, the concepts were evaluated in a Harrison profile and the most successful design was selected to be further optimized in the final concept.

2.2.1. The mesh

The mesh design was based on previous research which was done by other groups as a solution for recording epicardial signals (Appendix C). The concept consists of an elastic mesh in which the electrodes are evenly placed. An example of a mesh is given in Figure 2. In this design, an anatomical model of the heart was coated in an elastic material, e.g., latex or silicone. After the coating had cured, it was removed from the model and electrodes could be inserted.

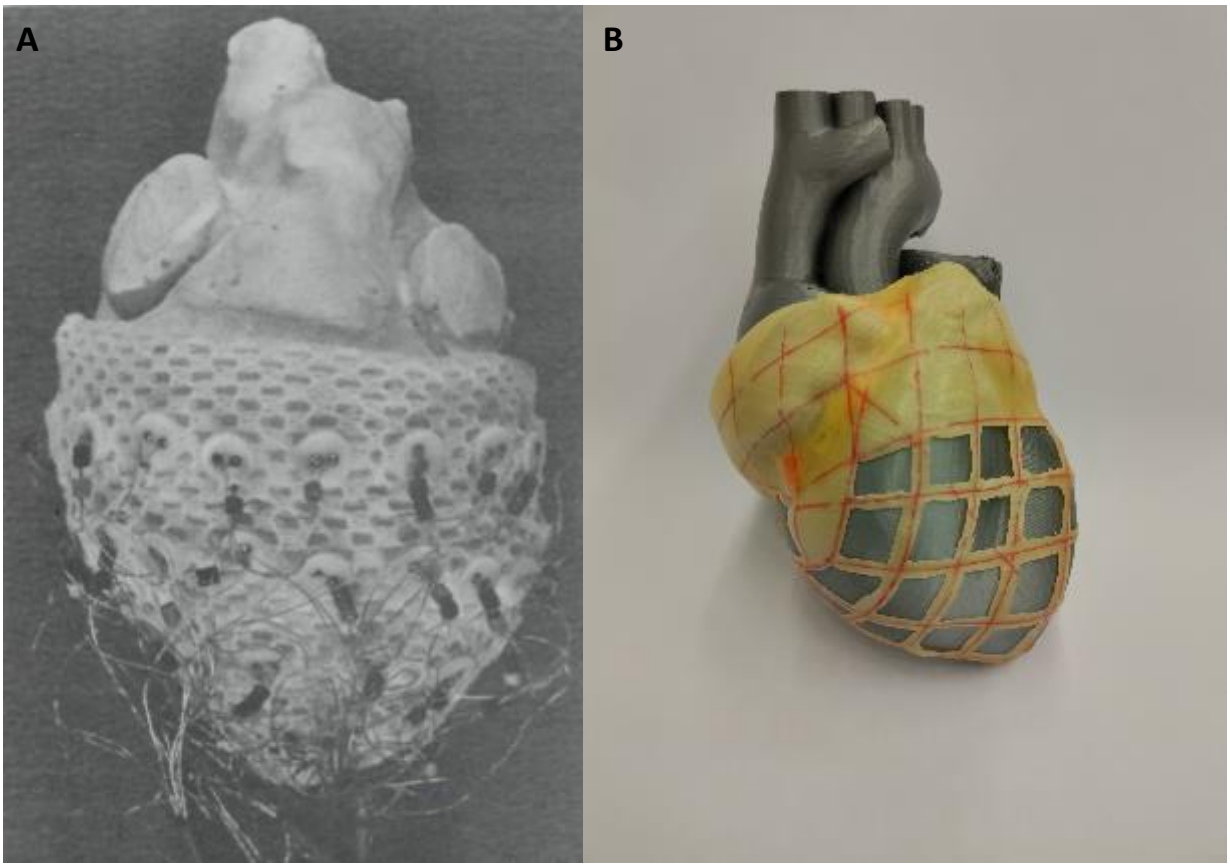

Figure 2. A. Design for the mesh electrode array used to record the electrical activity of canine heart. B. A concept for a mesh that uses a 3D printed heart as a mold with cut-out section for better visibility and reducing the stiffness of the mesh

2.2.2. The envelop

This design was a foldable sock (Figure 3). The concept behind this design was based on kirigami, a variation of origami where the paper is cut as well as being folded. From the heart, a cutout template was created, by suturing and folding the cutout in a specific pattern an epicardial sock was formed. The advantage of using this method was that the cutout can be easily manufactured since only a 2D design is needed. However, suturing the cutout around the heart was a challenge as many parts had to be stitched together, increasing the time that was needed to start recording the electrical signals. Finally, not all the locations that need to be sutured were easily reachable when placed around a heart.

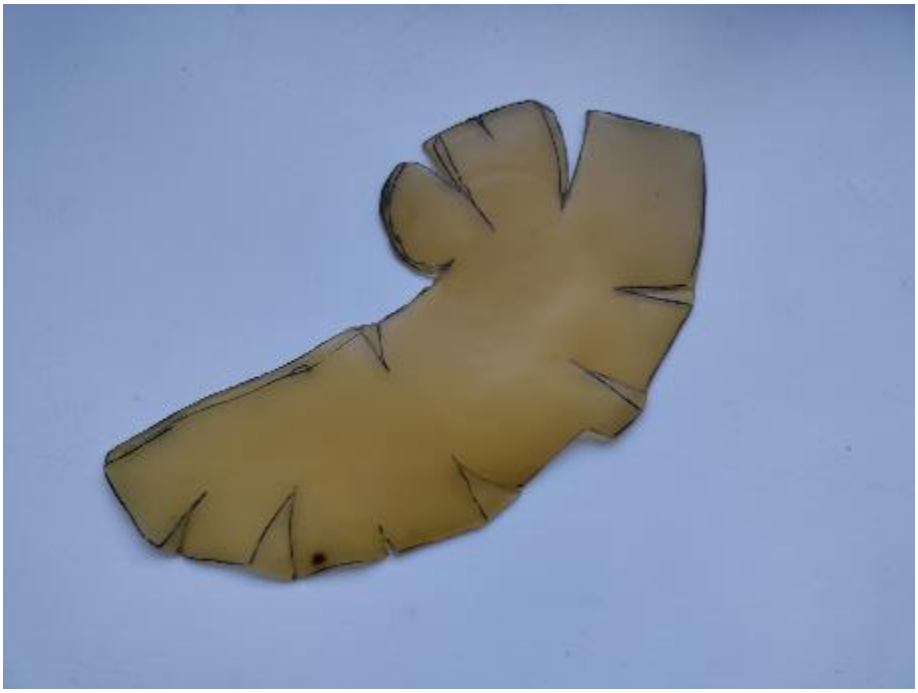

Figure 3. Concept design for an unfolded heart envelop by suturing the edges to each other, the cut-out will shape into a sock that can fit over the heart

2.2.3. The bag

This concept design is based on a burlap bag that can be tightened with a string. The principle behind this concept was that by pulling the strings, the sock would close and wrap around the heart. Similarly, to the previous design, the electrode array can be made from a flat material, thus making construction easy. The force the sock exerts on the heart can be controlled by which the string are pulled that was used to pull on the strings (Figure 4). Just like with shoelaces, pulling harder increases the pressure.

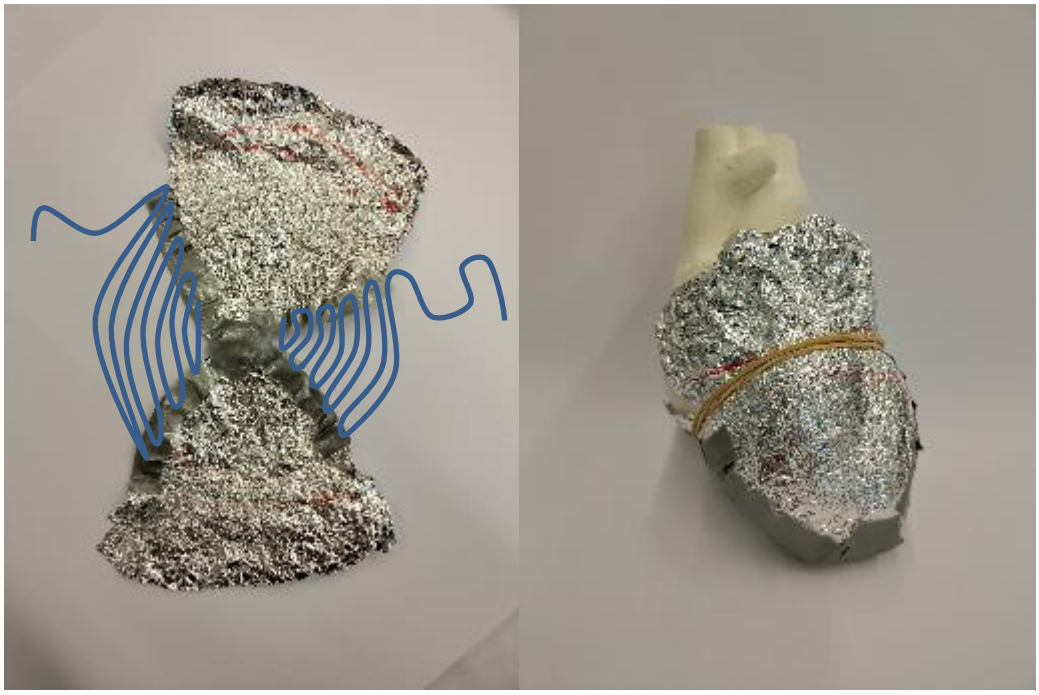

Figure 4. The bag design, by tightening the blue strings the sock will conform to the shape of the heart like a burlap bag.

2.2.4. The scarf

The concept of the scarf was based on wrapping bandages around the heart. The scarf was a long flexible flat electrode array. By wrapping this around the heart, the electrical activation could be simultaneously recorded (Figure 5). To cover the whole surface area of the ventricles, part of the scarf needed to overlap with itself which can cause noise in the signals. The main advantage was that the electrode array could be wrapped around the heart in multiple ways. However, this was also a limitation of the electrode array, as the locations of the electrodes on the heart was different each time.

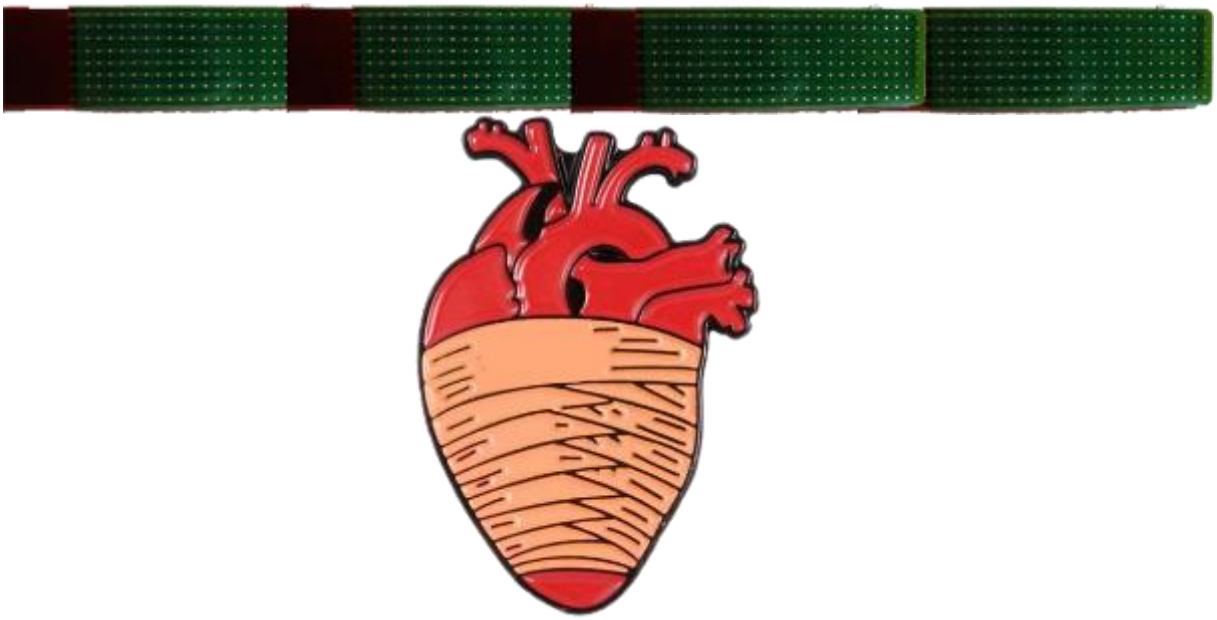

Figure 5. Top. Concept design for the scarf electrode array. Bottom. A visualization of how the scarf electrode array would be wrapped around the heart.

2.2.5. 3D printed sock

3D printing has becoming more popular and advancements in printing technology allows for multi materials printing. By utilizing these techniques, it becomes a possibility to print the whole epicardial sock, including electrodes. In this way, the complex geometry of the heart was used as a model for the sock. To reduce the force that was exerted on the heart, a special patterns was designed. This reduced the stiffness of the sock, and reduced the materials needed for 3D printing (Figure 6).

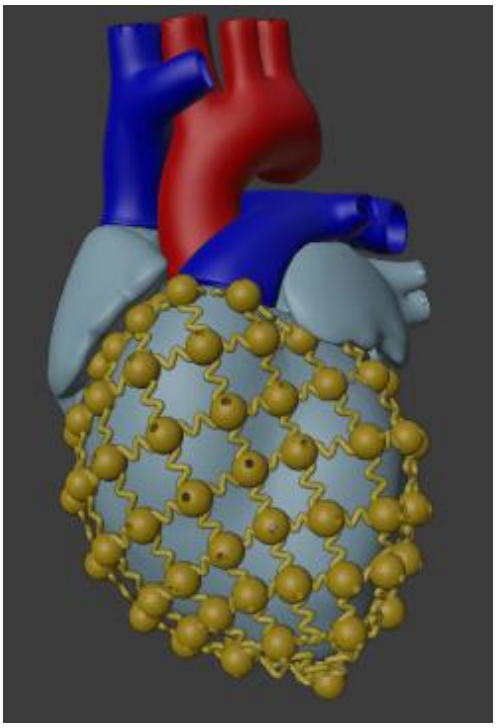

Figure 6. Concept art of how the sock is going to fit over the heart

2.3. Final concept

2.3.1. Harris profile

To select the most promising concept, a Harris profile was made for comparing the strength and weaknesses of each design regarding the requirements that have been established in section 2.1 (Table 1). In the Harrison profile, the importance of the requirements is ranked by their position, the top requirement is the most important and the bottom is the least important requirement. Each design was evaluated by the requirements and a ranking was given of --, -, +, or ++ depending on how well the requirement was met. After each requirement had been evaluated, the total score was calculated. The design with the highest score was used as the base for the electrode array and further optimized.

Heart impairment was graded based on the force it would exert on the heart. It was not possible to calculate the force exerted by the design, for these designs assumption was made on the exerted force on the heart. Electrode contact assessment was based on how well the electrode array would fit over the heart. The better the fit over the heart, the higher the score. Elasticity was scored on how easy it was to deform the sock. Ease of use was assessed on the number of actions it would take to put the sock over the heart and the time needed to record electrical activity. Transparency, was graded on the surface area that was covered by the sock, with more surface area being covered resulting in a lower score. Sterilizability was graded on how well the concept idea would be able to be sterilized. The score for high resolution was determined by the number of electrodes that could fit in the electrode array, the higher the number of electrodes, the higher the score. Electrode localization was graded on of the basis of how well the electrodes could be located on the heart. From the Harris profile, it can be seen that the 3D printed design had the best score. Therefore, it was chosen to be further developed into a working prototype in this study.

Table 1. Harris profile of the different concepts

	Mesh	Envelop	Bag	Scarf	3D print
Heart impairment	--	+	+	+	++
Electrode contact	+	-	-	-	++
Elastic	-	-	-	--	++
Ease of use	+	--	-	--	++
Transparancy	--	--	--	--	++
Sterilizability	+	+	+	+	++
High resolution	-	+	+	++	-
Electrode localization	++	+	+	--	++
Total	-	--	-	----	++++++++++++

2.4. Prototyping

2.4.1 Material

Elastomers are known for their ability to reach high elongations before failure [14]. However, 3D printing of elastomers remains difficult as the material properties of the elastomers brings unique challenges with it for each method of 3D printing. Elastic 50A resin (Formlabs Inc., Somerville, MA) was chosen as this elastomer was compatible with the 3D printer that was used, had a lowest ultimate tensile strength of the materials provided by the manufacturer (Formlabs Inc., Somerville, MA), and could be sterilized.

2.4.1. Stiffness of the sock

The most important requirement for the electrode array was the impairment of the heart function. The pressure that was exerted by the sock was estimated by modeling the sock as a spherical, thin-walled pressure vessel. The pressure was calculated with [13]:

$$\sigma = \frac{P*r}{2*t} \qquad \text{Eq. 1}$$

Where σ is the stress in the wall, P is the pressure, r is the inner radius of the sphere, and t is the wall thickness. From the literature, it was found that the volume of the heart between diastole and systole changes by 8%. The sock conforms to the heart, as the heart changes in size, so does the sock. With Hooke's law, the stress can be calculated with the strain of 8% [8].

$$\sigma = \mathrm{E}\varepsilon \qquad \text{Eq. 2}$$

The sock was modeled as a perfect sphere. This gives:

$$\varepsilon = \frac{r}{r_0} - 1 \qquad \text{Eq. 3}$$

Where r_0 is the original radius of the sphere and r is the radius after deformation. As the sphere deforms, the thickness of the wall will change. The new thickness can be calculated using Poisson's ratio (v). Assuming the material used for the sock behaves like a rubber, v for rubbers is typically 0,5, meaning the volume remains constant. This gives:

$$r^2 t = r_0^2 t_0 \qquad \text{Eq. 4}$$

Rewriting Eq. 4

$$t = t_0 \left(\frac{r_0}{r}\right)^2 \qquad \text{Eq. 5}$$

By combining Eq. 1,2,3 and 5 gives

$$P = \frac{2E(r-r_0)t_0 r_0}{r^3} \qquad \text{Eq.6}$$

Assuming the max pressure of 2.7 kPa and the spherical model of the heart with r_0 = 6 cm, t_0 = 2 mm and ε = 0.08, an estimation can be made for the maximum value of Young's modulus the sock can have, which is 0.63 MPa.

2.4.2. Pattern design

It is well known that the structural design of the material can help release stress and minimizes the strain in a localized point, and therefore make the material more stretchable [15]. To accommodate for the large strains, patterns like serpentine, meanders, horseshoe, and spirals have been designed [26]. How well these patterns can dissipate the stress by the induced strain is dependent on the shape, length and curvature of the pattern [15]. For this prototype, a wave-pattern was chosen for its well-known ability to dissipate the stress. For minimal stress in the material, the width of the wave-pattern should be as small as possible [29]. When the wave pattern was stretched, the stress experienced in the bends of the pattern can be estimated with the curved beam equation (Eq. 7 and 8). Estimating the radius of the curve (r_c) and using the radius of the beam (r) gives:

$$\sigma_i = \frac{M}{eA}\left(\frac{c_i}{r_i}\right) + \frac{F}{A} \qquad \text{Eq. 7}$$

And

$$\sigma_o = -\frac{M}{eA}\left(\frac{c_o}{r_o}\right) + \frac{F}{A} \qquad \text{Eq. 8}$$

Where M is the moment, e is the distance between r_c and the neutral axis, r_i is the radius of the inner wall, c_i is the distance between the neutral axis and r_i, and F is the force exerted on the beam. r_o is the radius of the inner wall, c_o is the distance between the neutral axis and r_o.
The moment was calculated from:

$$M = F * d \qquad \text{Eq. 9}$$

With d half the width of the wave pattern. From Eq. 7 and 8 it can be seen that as the radii of the bends decreased, the stress increased. With repeated stretching, it eventually resulted in failure of the wave pattern. Therefore, to reduce the stress and chance of failure, a wave-pattern with a large internal radius at the peaks and valleys of the pattern was recommended (Figure 7).

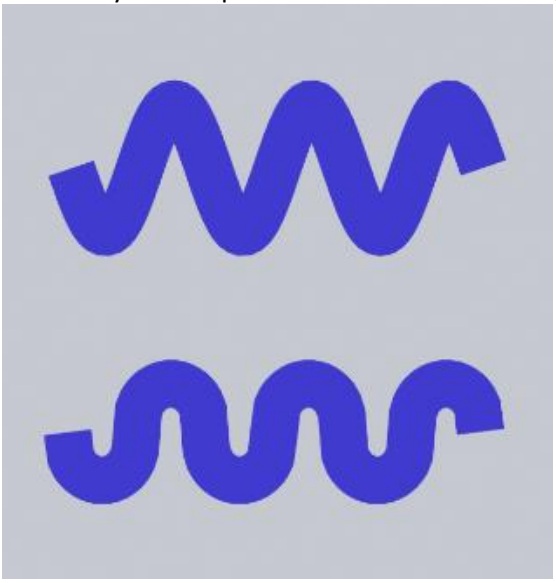

Figure 7. Wave pattern with different internal radii. Top: standard sine wave. Bottom: modified sine wave with a larger radius.

2.4.3. Electrodes

To record the electrical activation on the epicardium, old catheters were saved and repurposed to fit into the sock. Old catheters were chosen to limit the cost of building a prototype and to reduce the waste. In the design of the sock for the electrode array, special holes were created that could fit a catheter tip. Catheter tips were inserted into the holes and fixated with glue (Pattex lijm 100% All-Purpose glue, Henkel Nederland B.V., Nieuwegein, The Nethelands) In total 37 electrodes were used for recording the electrical activation.

2.4.4. Localization

The electrodes were localized with the help of the pattern that was designed for the sock. The electrodes that were aligned with the anatomical locations of the heart, were projected on a 3D model of the heart. By matching the corresponding electrodes of the model to the electrodes of the electrode array, all the electrodes can be localized on the heart model.

3. Methods

3.1 Sock design

3.1.1. Fabrication of the test strips

To investigate the effect of the pattern on the stiffness, three different wave patterns were designed of 140 mm by 30 mm, with a varying thickness. Pattern 1 was a normal sine wave with an amplitude of 2 and a length of 3 wavelengths, Pattern 2 was a modified sine wave with an amplitude of 0.5π and a length of 3 wavelengths. The third pattern was a modified sine wave with an amplitude of 0.5π and a length of 2 wavelengths (Figure 8). Samples were 3D printed with a thickness of 1.5 mm, 2.0 mm, 2.5 mm, and 3.0 mm. A section of 10 mm, at each end of the test strip, was designed to be able to hold the test strips in the mechanical jaws of the test machine. After printing, the test strips were removed from the build plate and post-processed. The samples were visually inspected for inconsistencies and flaws like broken interconnections. In total 2*3*3*4 = 72 test strips were printed.

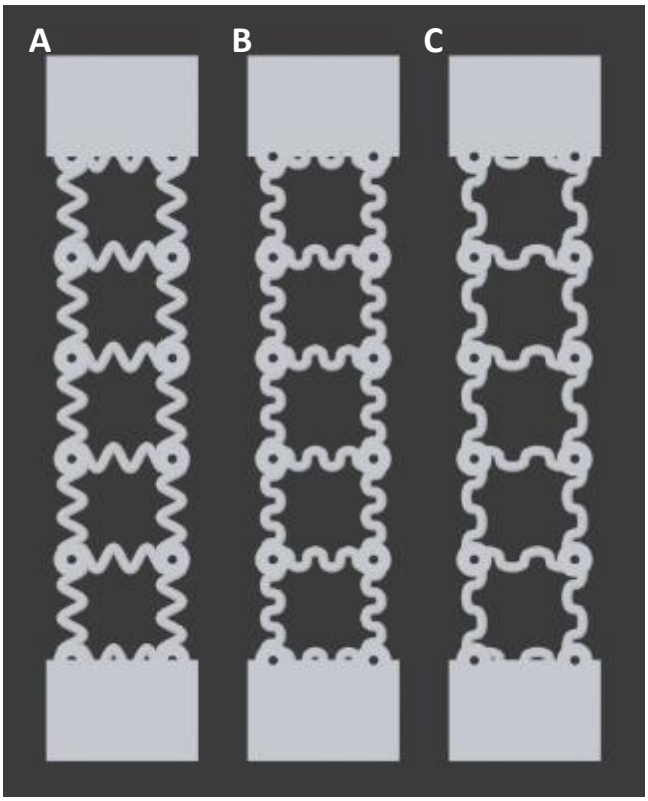

Figure 8. The designs of the test strips. A. Pattern 1, B. Pattern 2, C. Pattern 3

3.1.2. Tensile test

Tensile tests were performed on a ZwickRoell Z010 tensile tester with a load cell of 500 N at room temperature. The test strips were clamped in the flat jaws of the machine without any pre-stretch. A mark at the edge of the clamps was made on the specimen to visualize for slippage of the specimen. The test strips were loaded at a rate of 60 mm/min until a load drop of 10% of the maximum force was detected. During testing, the elongation and the force were recorded and plotted against each other. The strain was calculated from:

$$\varepsilon = \frac{l - l_0}{l_0} \qquad \text{Eq. 10}$$

Where and l_0 = 140 mm and l is the length of the elongation. From the tensile test results, the maximal tensile stress can be found from:

$$\sigma = \frac{F}{A} \qquad \text{Eq. 11}$$

Where F is the applied force and A is the surface area. As the stress in the samples applied in parallel with the wave patterns, the formula for A was simplified to:

$$A = 2 * \pi * r^2 \qquad \text{Eq. 12}$$

Combining Eq. 11 and 12 gives:

$$\sigma = \frac{F}{2 * \pi * r^2} \qquad \text{Eq. 13}$$

The stress and strain were plotted against each other and the apparent Young's modulus (E_a) was calculated by determining the slope of the stress strain curve. E_a is an approximation for the stiffness of the wave pattern and not the stiffness of the material itself. Eq. 6 was used to calculate the maximum value for E_a the sock could have at each thickness (Table 2).

Table 2. Estimation for maximum E_a from eq. 6

Thickness	Estimation for E_a [MPa]
1,5 mm	0,630
2,0 mm	0,472
2,5 mm	0,378
3,0 mm	0,315

3.1.3. Fatigue test

Cyclic loading is the can result in fatigue cracks, which over time eventually would lead to failure of the sock. For an estimation of the fatigue life of the sock, fatigue tests were performed on a ZwickRoell Z010 tensile tester with a load cell of 10 kN. The test strips were clamped in flat jaws and a mark was made on the test strip, at the edge of the jaw. The strips were elongated by 20 mm at a speed of 16 mm/s and then brought back to the original length at a speed of 16 mm/s. This was repeated for 1000 cycles or until failure of the test strip. One cycle was defined as the elongation of the sample and relaxation of the samples. Failure was defined by breaking of two or more connections between the intersections. All tests were performed at room temperature.

3.2. Fabrication of the electrode array

A 3D heart model provided by the Erasmus MC (Figure 9A), was used as the base for the design of the sock. Blender (Blender 2.93.6, Blender Foundation, Amsterdam, The Netherlands) was used to visualize the model and to create the sock design. In blender, a sphere was projected onto the ventricular surface. This geometry was used to create the wave pattern with the help of a custom made python code (Appendix A). The python code subdivided a edge in 128 sections and displaced each section according to the mathematical formula of the wave pattern, in this study a modified sine wave was used. On the vertices of the sphere, points in 3D space that create the geometry, smaller spheres with a radius of 3.5 mm were created at each vertex (appendix A) and hole with a radius of 1 mm was made in each sphere. The model for the sock was imported into Preform (Formlabs Inc., Somerville, MA) (Figure9B). For unsupported regions of the model, extra support was generated using the auto-generate option. The parameters used for the support were mini rafts, at a density of 1.0, and touchpoint size of 0.5 mm. The model was automatically sliced at a layer thickness of 0.1 mm resulting in a total layer count of 1115 layers. A project file was created that could be imported into the 3D printer (Form 3,Formlabs Inc., Somerville, MA). The model was printed in flexible 50A resin (Formlabs Inc., Somerville, MA). After printing the model was washed for 10 minutes in a washing machine (Form Wash, Formlabs Inc., Somerville, MA) on the build plate, and then 10 minutes in a basket. Then the model was fully cured for 20 minutes at 60 ˚C in an ultraviolet chamber (From Cure, Formlabs Inc., Somerville, MA) (Figure 9C). Finally, the remaining support material was removed by hand Figure 9D).

Tip of the catheters were cut off and soldered to a 2-meter-long wire. Each recording electrode was tested for continuity before it was fixated in the sock. In total 37 electrodes were fixated onto the sock. The electrodes were connected to an amplifier (EP WorkMate™ Signaling conditioning unit, St. Jude Medical) by an EP WorkMate™ 56-pin one piece catheter interface (Figure 10)

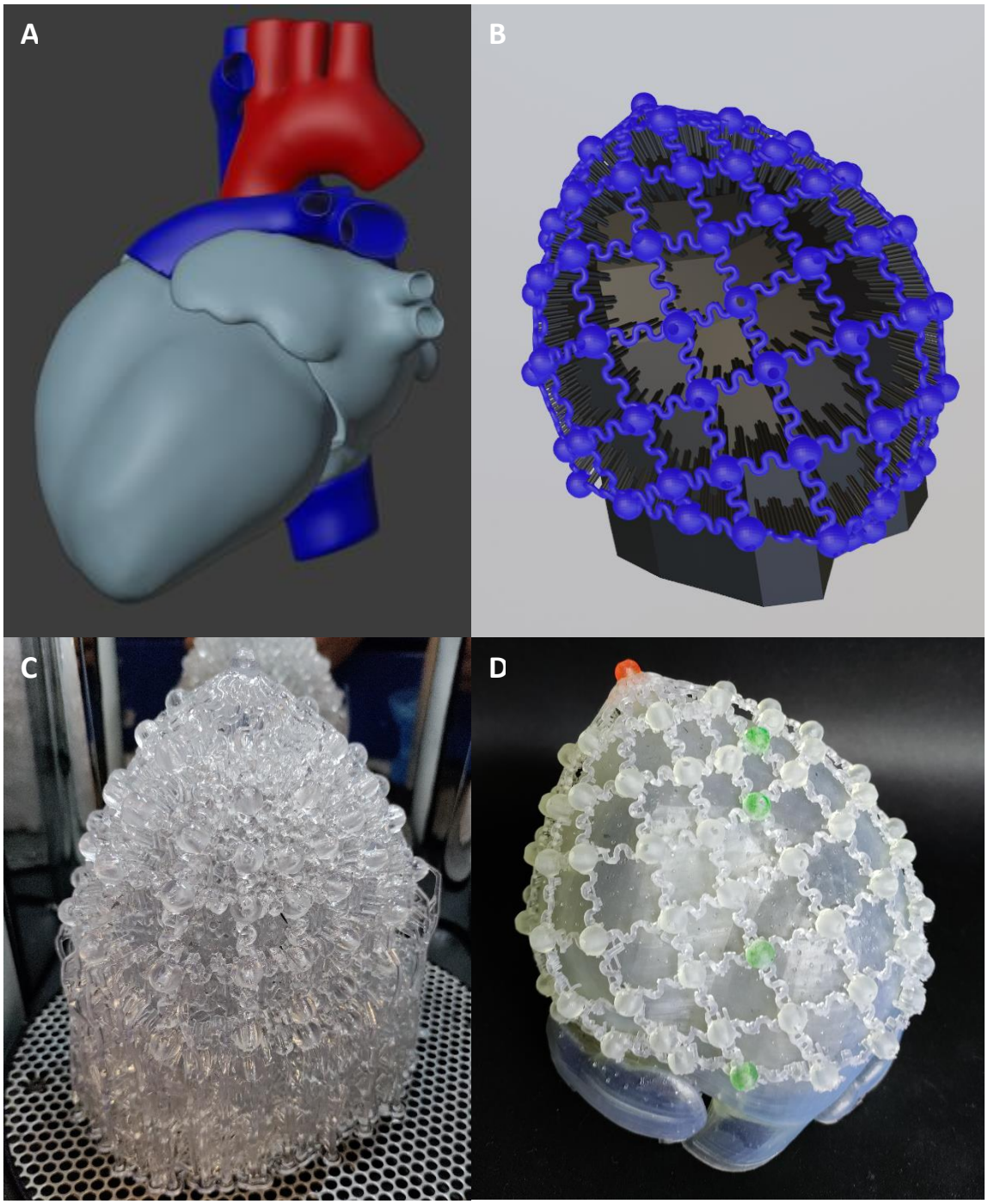

Figure 9. Different stages of the design of the sock. A. Anatomical model of the human heart provides by the Erasmus MC. B. The 3D model of the sock design and support structure that was imported into the slicer software. C. 3D printed sock with the internal support still attached. D. The sock with the support material removed on a 3D printed model of the ventricles.

3.3 Data acquisition

3.3.1. Study population

To test the functionality of the electrode array, slaughterhouse porcine hearts were obtained from the abattoir according to the protocol developed by the Erasmus MC [1]. The excised heart was prepared to be placed in a EVHP setup. A metal wire was wrapped around the ascending aorta as a grounding electrode for unipolar recordings.

3.3.2. Mapping procedure

Two pacing electrodes were stitched into the left and right ventricular wall, and the heart was stimulated at 80 beats per minute. After successful resuscitation of the porcine heart, the electrode array was placed over the heart, and the electrode array was aligned on the heart with the apex, posterior interventricular artery and the crux cordis. The indifferent electrode was attached to the metal wire. Unfiltered electrical activity was recorded for 5 seconds, sampled at 2 kHz and saved on a hard disk of the computer to be later analyzed.

3.3.3. Data analysis

The data was analyzed using custom-made software. The activation times were derived from the recorded electrograms by annotating the steepest part of the negative slope of the electrical signal recorded by each electrode. The total activation time (TAT), was calculated from the time between the onset of the first activation and the last activation measured by the sock in one heartbeat. A 3D color coded activation map was created from the activation times and the location data of the electrode array. Areas where no electrical activation was recorded were indicated by leaving the electrode location intentionally black.

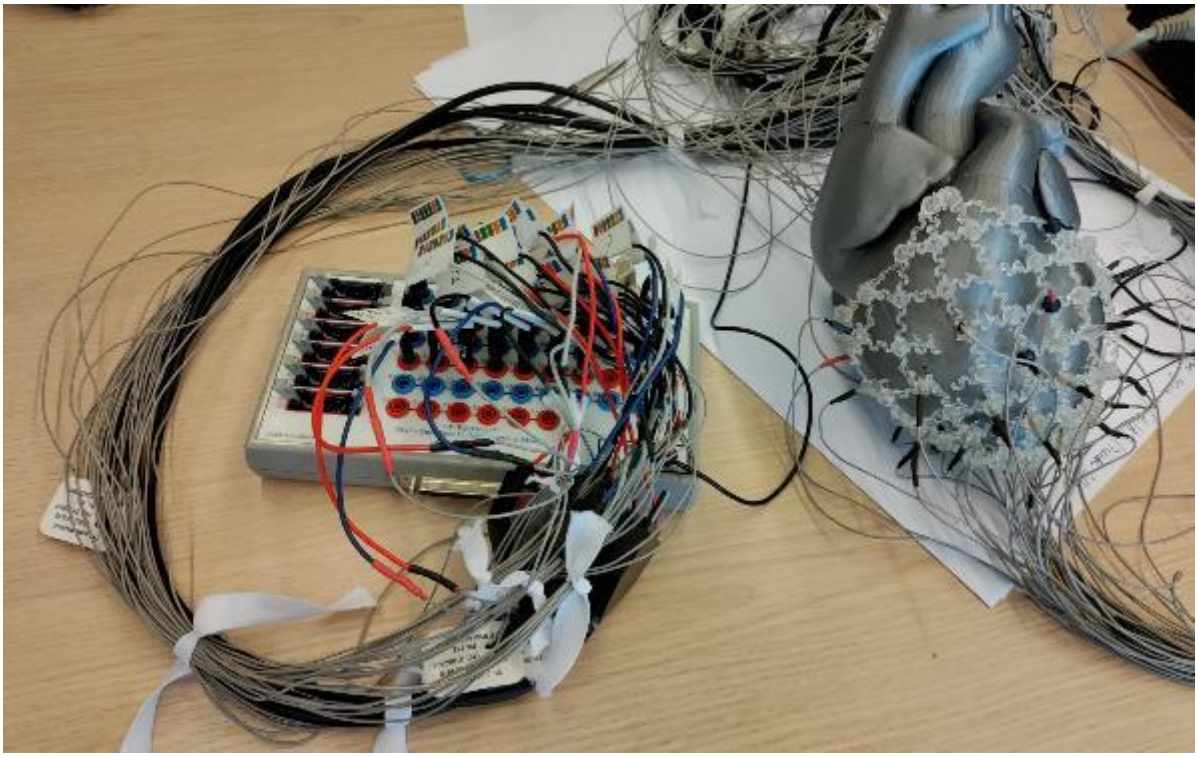

Figure 10. The electrode array over a 3D printed model of the heart and connected to the EP WorkMate™ 56-pin one piece catheter interface

4. Results

4.1. Testing

4.1.1. Tensile test

From the tensile test data, stress-strain curves were plotted (Figure 11) and the slope of the stress-strain curve was calculated between 0.016 and 0.15 strain (Table 3). In section 3.1.2. an estimation was calculated for the maximum allowed E_a for the different thicknesses (Table 2). It was found that only Pattern 1 with a thickness of 1.5 mm was below the maximum E_a. For Pattern 2 and 3, the E_a was higher than the estimation. It can be seen that E_a was affected by the shape of the pattern and the thicknesses. At a thickness of 1.5 mm, E_a for each pattern was different. With an E_a of 0.61 MPa, 0.65 MPa, and 1.0 MPa for Patterns 1, 2, and 3 respectively. As the thickness of the samples increases, the rate at which E_a increases was different for each pattern. The change in E_a, as the thickness increases was the largest for Pattern 1, 1.2 MPa, for Pattern 2 and 3 this is 0.63 MPa and 030 MPa respectively.

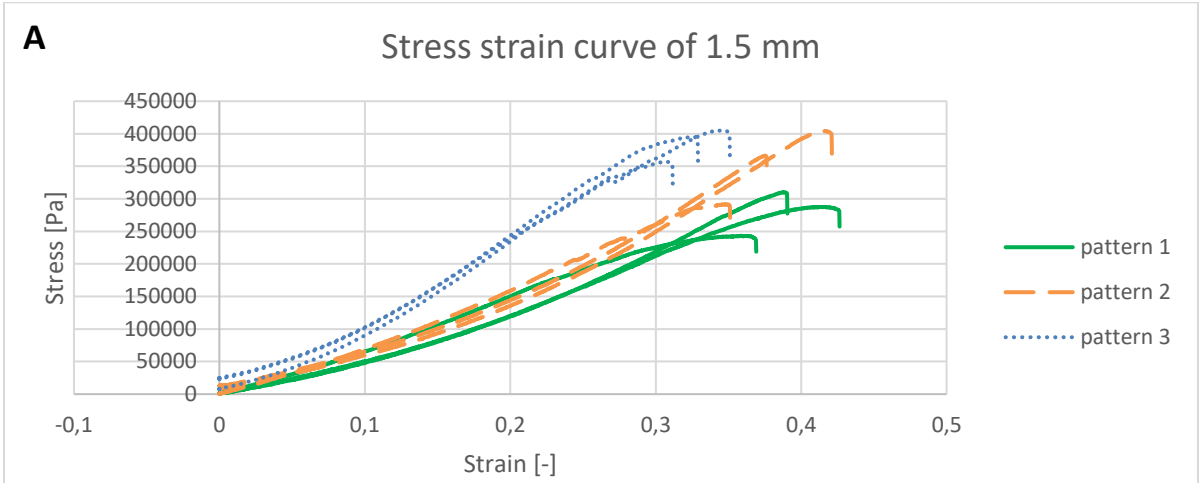

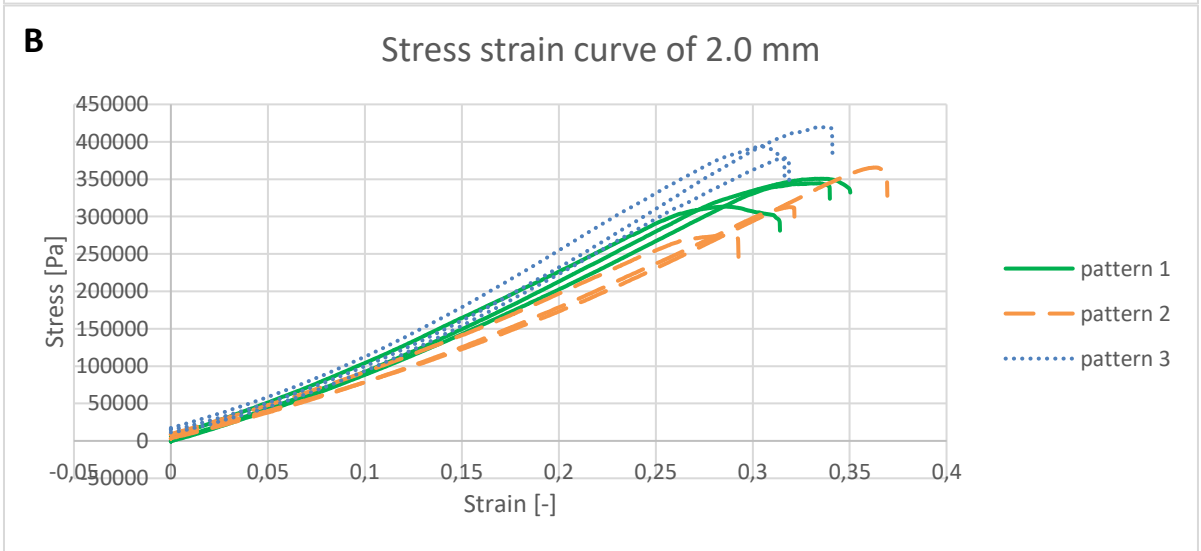

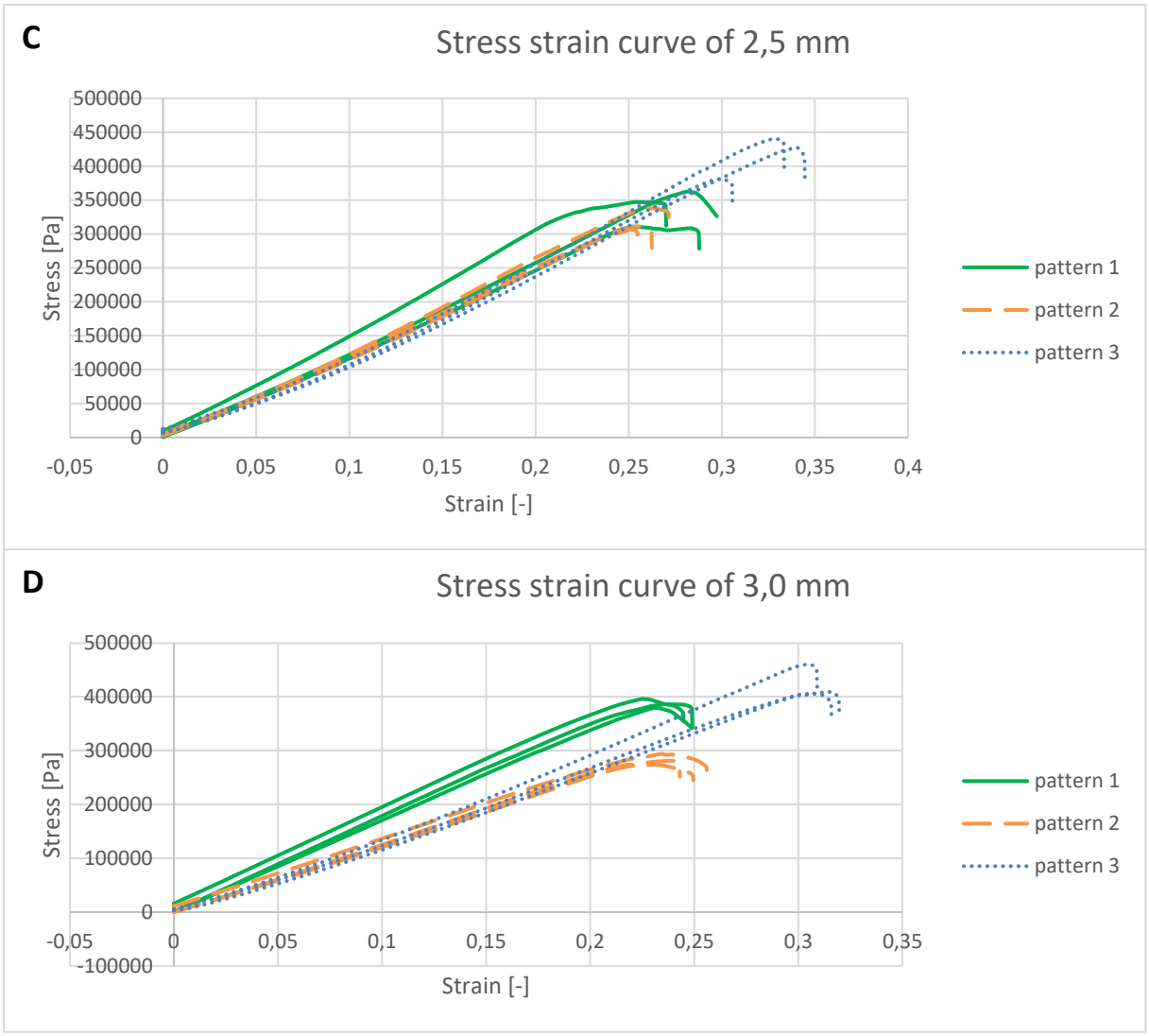

Figure 11. stress strain curves obtained from the tensile test. A. are test results of the test strip with a thickness of 1,5 mm. B. are the test results of the test strips with a thickness of 2,0 mm. C. are test results of the test strip with a thickness of 2,5 mm. D. are test results of the test strip with a thickness of 3,0 mm.

Table 3. Mean of experimental results

	Pattern 1		**Pattern 2**		**Pattern 3**	
	E_a [MPa]	Fatigue test Cycle [-]	E_a [MPa]	Fatigue test Cycle [-]	E_a [MPa]	Fatigue test Cycle [-]
1.5 mm	0,608±0,0944	236±120*	0,652±0,0931	285±79,1	1,02±0,0231	274±61,2
2.0 mm	1,03±0,0511	125±28,0	0,841±0,0553	132±110	1,05±,0599	272±39,1
2.5 mm	1,30±0,139	33±11,3	1,23±0,0535	35±31,0	1,15±0,0332	190±85,1**
3.0 mm	1,76±0,0450	14,7±2,52	1,28±0,0256	43±14,8	1,32±0,0748	138±65,0

**one sample was reused after a fatigue test of 100 cycles at 15 mm of elongation. ** total sample size of 2*

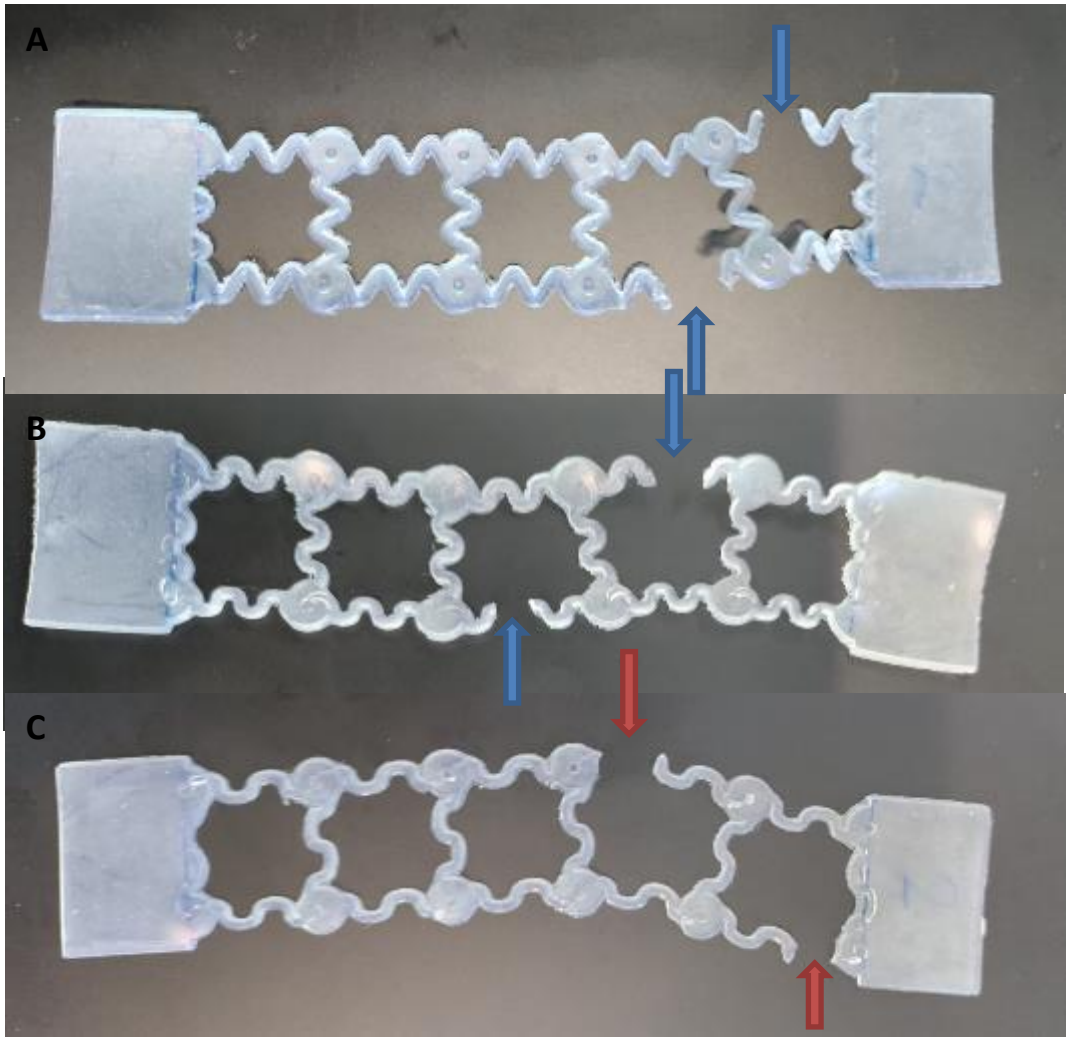

Figure 12. Failure points of samples. A. pattern 1 - 1,5 mm thick. B. pattern 2 - 1,5 mm thick. C. pattern 3 - 1,5 mm thick. The blue arrows point to the location of failure in the wave pattern. The orange arrows point towards the location were the wave pattern connect to the intersections.

4.1.2. Fatigue test

Fatigue life of 35 samples were tested on a ZwickRoell Z010 tensile tester with a load cell of 10 kN. Table 3 shows that the samples break at an earlier stage as the thickness increases. At a thickness of 2.0 mm and higher, Pattern 3 has a longer fatigue life when compared to Patterns 1 and 2 for the same thickness. The location of failure of the test samples were located at the location where the internal radius of the pattern was the smallest. For Patterns 1 and 2 the location of failure was in the bends of the wave pattern. In Pattern 3 it was at the location where the wave pattern connects to the electrode location (Figure 12). At the locations where the radius was the smallest, the stress was high which resulted in the failure of the pattern.

4.1.3. Experimental test

The prototype

The prototype used in the experiments consisted of a sock with wave Pattern 2 (Figure 13A). Electrodes were inserted in the holes of the intersections, to create the electrode array (Figure 13B). In total 2 experiments were performed with the sock, the first experiment did not contain any electrodes (Figure 13A). The second experiment was performed with a sock that contained the electrodes (Figure 13B). While the heart was beating, the sock was easily placed around the heart. It was observed that the wave pattern of the sock was visually expanding without observing changes in the contractions of the heart. In the first experiment, the sock showed no movement from its position during contractions. However, in the second experiment, the sock needed to be fixated with the help of suture wires that were attached to the superior part of the sock and the container of the EVHP setup. The weight of the electrode wires were pulling the sock of the heart. After the removal of the sock, it was noted that several wave patterns had failed. These failures did not had a significant impact on the function of the sock, depending on the position of failure.

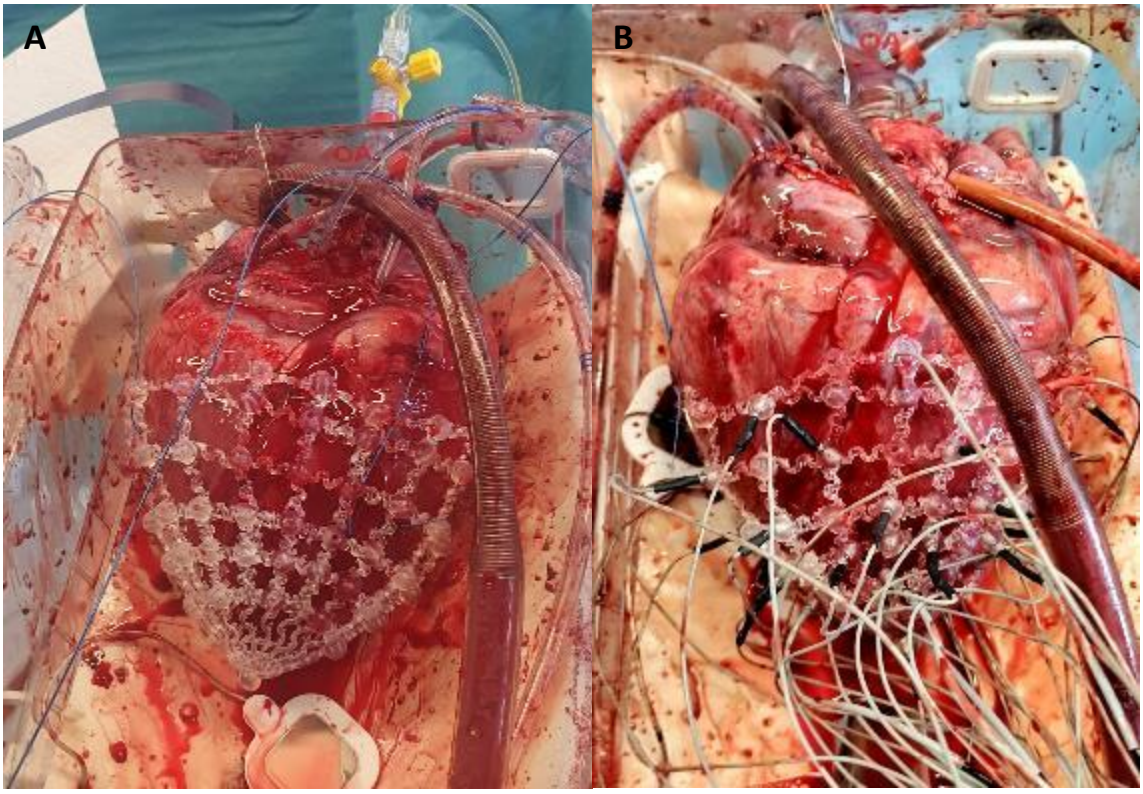

Figure 13. A. The sock on a pig heart without any electrodes. B. The sock with electrodes attached on a pig heart

Mapping

Five second unipolar recordings were made of the of electrical activity (Figure 14). In total two activation maps were generated (Figure 15). In the first activation map, the heart was paced from the LV (Figure 15A), in the second activation map the heart was paced from the RV (Figure 15B). It can be seen from Figure 15A, as the heart was paced from the LV, the electrical activation travels from the LV to the RV. When the heart was paced from the RV, the signal travels from the right side to the left side. TAT was 188.5 ms and 196.5 ms when paced from the LV and RV respectively.
Unfortunately, not all electrodes that were connected to the recording system measured an activation peak in the signal. Of the 37 electrodes, 6 electrodes did not record a signal, and were therefore excluded from the activation maps.

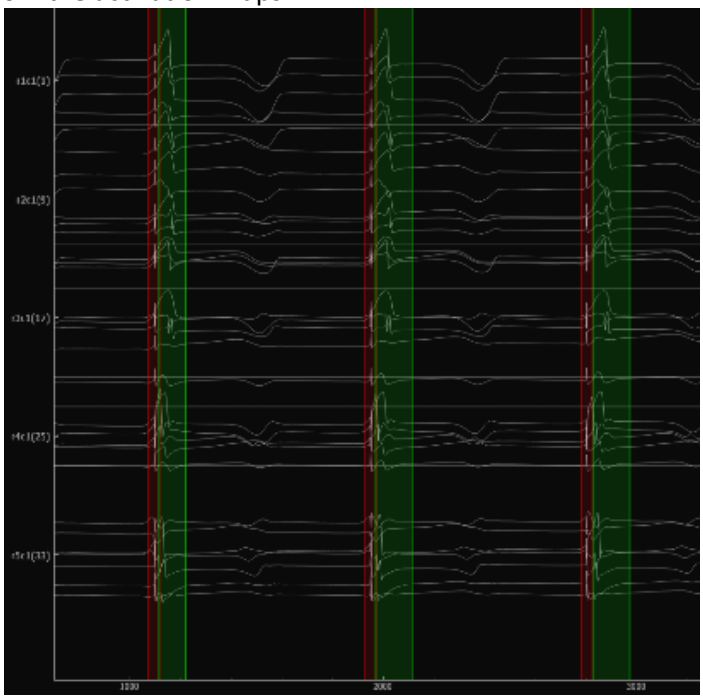

Figure 14. Raw mapping data. The red bars show the activation spike of the pacemaker. The green bars indicate the activation signals.

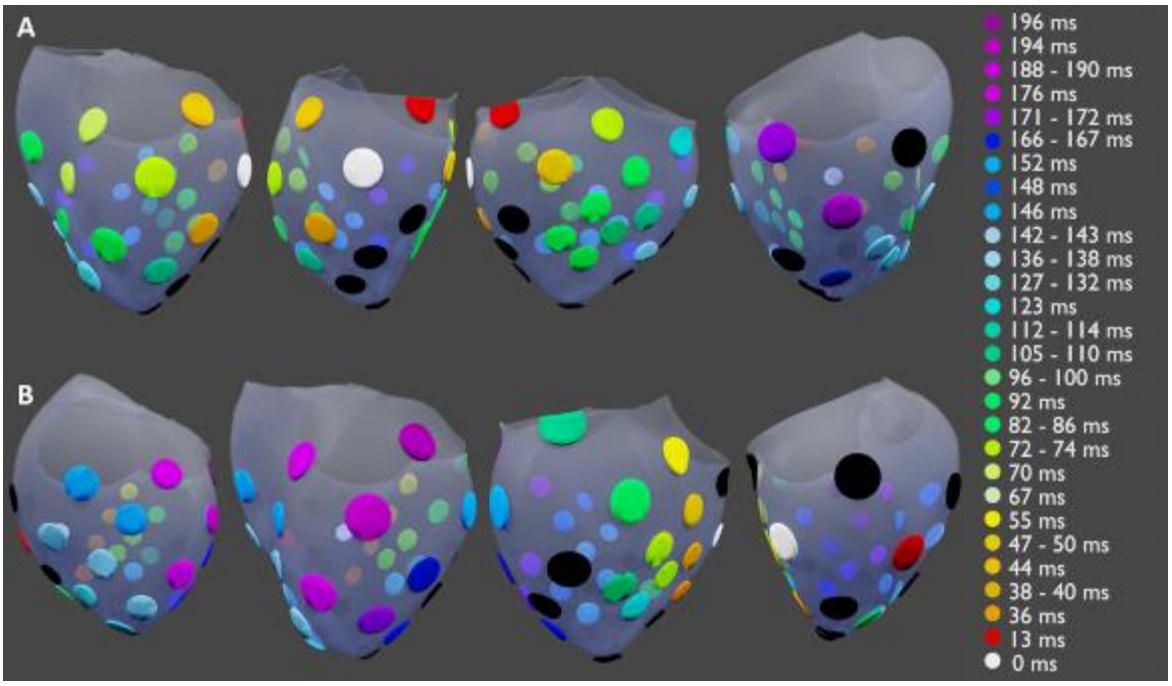

Figure 15 A. Activation map when paced from the right ventricle at 80 bpm. B. Activation map when paced from the left ventricle at 80 bpm. The black dots are the locations where no activation is measured.

5. Discussion

This is the first study that has developed a 3D printed electrode array the can record the electrical activity of the ventricular surface simultaneously. The findings of this study show promising results for simultaneously recording the electrical activity of the ventricles. The activation maps obtained from the electrode array allow to determine the direction the electrical wave propagates over the ventricles, and TAT of one heart cycle. In this section the results of the tensile test, fatigue test and the proof-of-concept test are discussed. The limitations and the future prospects of the study will also be discussed.

5.1. Findings

5.1.1. Tensile test

From the tensile test, it was found that E_a is dependent on the shape of the pattern and increases with the thickness of the samples. As the thickness of the samples increased, the inner radius of the wave pattern decreased (Figure 16) and the pattern was more resistant to deformation when stress was applied. This causes the pattern to approach the Young's modulus of the material, instead of the pattern. Furthermore, the decrease of the inner radius of the pattern increased the stress experienced at these locations. As the stress increased, the material started to tear due to the stress concentrations resulting in failure at lower strains. This was observed in the difference in strain between Pattern 2 and 3. Pattern 3 is similar to Pattern 2, but only differs in the number of waves between two intersections. Pattern 3 consisted of fewer waves, as the thickness of the sample increased the wave pattern did not fuse together. Therefore, as the pattern was stretched out, the stress on the inside of the bend was lower than for Pattern 2. Due to the lower stress in Pattern 3, higher strain values were measured before the samples failed, when compared to Pattern 1 and 2. The goal of the tensile test was to investigate the effect of the pattern and thickness on E_a, where a pattern scored better for a lower E_a. Meaning, the pattern could easily be deformed. The results in Table 3 shows that Pattern 1 with a thickness of 1.5 mm was the best design for reducing E_a of the sock.

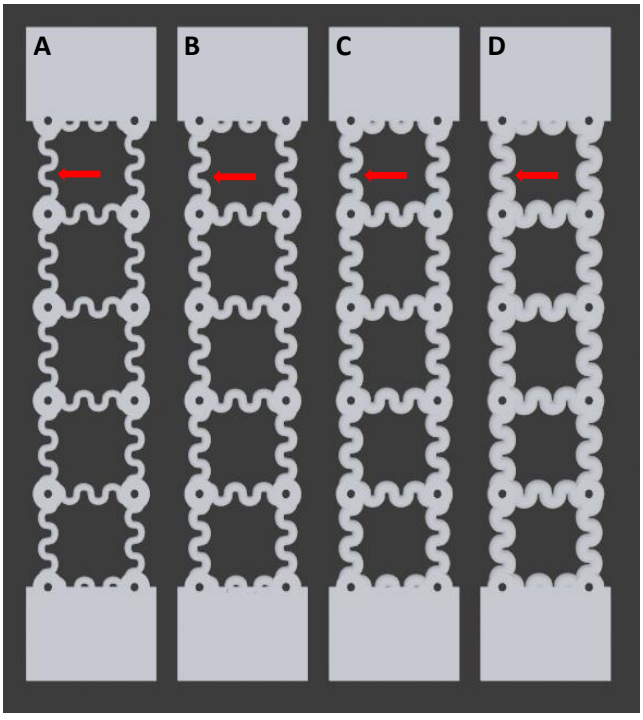

Figure 16. Visualization of the different thicknesses of Pattern 2. A. 1.5 mm. B. 2.0 mm. C. 2.5 mm. D. 3.0 mm. The red

5.1.2. Fatigue test

Data from the fatigue test was analyzed to investigate the effects of the thickness of the pattern on the fatigue life. Samples started to fail at fewer cycles as the thickness increased (Table 3). The increase in thickness resulted in a decrease of the inner radius of the bends in the wave pattern. As the samples were stretched to 0.2 strain, the stress at these locations increased to initiate a tear. After many cycles, the tear slowly propagates through the material until it completely fails. Pattern 3 only failed where the wave pattern was attached to the intersections (Figure 12C). The radius that was formed from the connection was smaller than that of the wave pattern. Patterns 1 and 2, failed most often at the bends of the wave patterns and not at the connections (Figure 12 A and B). These observations are following Eq. 7, which shows that the stress on the inside of the bent is affected by the inner radius. At greater thickness, the difference in cycle length before failure can be seen in Pattern 3 when compared to Patterns 1 and 2, as it can withstand significantly more cycles before failure. To increase the fatigue life of a pattern, the best method of achieving this is by reducing the inner radii of the wave pattern. This is why Pattern 3 has a higher fatigue life at a greater thickness when compared to patterns 1 and 2. The beating heart constantly exerts a strain on the sock. A design pattern with a low fatigue life would result in earlier failure of the electrode array, making the electrode array unusable. In the fatigue test, the higher the number of load cycles, the longer the fatigue life of a pattern. The results in Table 3 show that Pattern 2 with a thickness of 1.5 mm was the best design for increasing the fatigue life of the sock

5.1.3. Prototype design

After analyzing the results of the tensile and fatigue test, a decision was made for the pattern and thickness of the sock. From the tensile test, Pattern 1 with a thickness of 1.5 mm was the only pattern that was below the maximum calculated E_a of 0.63 MPa. However, in the fatigue test, Pattern 1 had the lowest fatigue life of all the tested patterns. As the selection of the wave pattern of the sock was dependent on both the fatigue test and tensile test, it was decided to use Pattern 2 in the prototype.

With the electrodes fixated in the sock, the electrical activity could be recorded and processed. In the second experiment, it was observed that the sock would slowly slide off the heart as a result of the added weight of the electrode wires. This prevents electrodes from making contact with the epicardial surface. A reduced weight of the cable would decrease the pull of the wires thus keeping the sock in place.

5.1.4. Requirements

For the development of the proof of concept, not all requirements could be met. There were many different path that could be taken, but this study focused on the feasibility of the design. This could be later further developed so the design would meet all the requirements. In the design of the sock, the pattern that was used, had an E_a that was higher than the maximum calculated E_a. During the experiments the ventricles did not collapse under the pressure exerted by the sock. The assumptions used in the design of the sock could have been too simplistic. The heart is a complex system and the movement during contractions are not uniform. This could have resulted in lower forces that were exerted on the heart.

It was noted that several connections between the electrodes had failed while the sock was over the heart. This failure of the pattern was due to the fatigue damage building up over time as the heart was beating. In most cases, this failure had no significant effect on the function of the electrode array, as surrounding connections would keep the electrodes in place. However, there was only significant failure when one of the superior connections broke. There were no surrounding electrode connections that could hold the sock together.

With the promising results obtained for the functionality of the sock, it is necessary to further investigate the use of different materials, the effects of the pattern on the durability, and E_a of the sock to reduce failure of the connections between the electrodes. In this study, sterility could not be achieved as not all components of the electrode array could be sterilized without damaging the components. However, the resin used for 3D printing the sock is a material that can be sterilized [9].

Due to sliding of the sock, the precision of the electrodes could not be accurately determined. High resolution recording in this study was not possible as the design of the sock pattern did not allow for more electrodes and the system that was used for recording the electrical activity could only process a small number of electrodes.

5.1.5. Mapping

It was decided to use unipolar recordings as these signals contain more information about the electrical activation, and it was possible to convert the unipolar recordings to bipolar recording if necessary (Appendix C). During analysis of the recordings several electrodes did not record a signal. This was caused by the pulling of the electrode wires, the sock would fold into itself, causing several electrodes to lose contact. It most often happened at the lateral locations of the heart (Figure 15).

The electrode array was able to identify the different propagation directions of the activation wavefront(Figure 15). As the heart was paced from the LV, the activation maps showed the electrical activation propagating from the LV to the RV. When the heart was paced from the RV, the direction of electrical activation was from the RV to the LV. By observing the activation patterns of the heart, a better understanding of the conduction pathways can be gained [24]. However, the sock was only able to make low resolution activation maps. The information that can be gained from this was limited to the direction of the activation wave, time after initial activation, and TAT.

The TAT times found in this study of 188.5 ms and 196.5 ms, was comparable to the results found in by Jurak [15]. Unlike this study, these porcine heart were excessed from anaesthetized pigs and the TAT were approximately 190 and 130 ms [4]. Even though the methods for acquiring the porcine hearts were different, the similarities in the TAT support the possibility to use the electrode array as a tool for identify the location of initial activation, TAT, and the direction of propagation of the activation wave.

5.2. Limitations

The results from this study were obtained with some limitations. During printing of the test strips, the test strips with a thickness of 2,0 mm and higher had area's where the pattern was filled in by the printer (Figure 17). This material was removed before the tests. However, during removal of the material, the pattern could have been damaged or altered and thus giving misleading results.

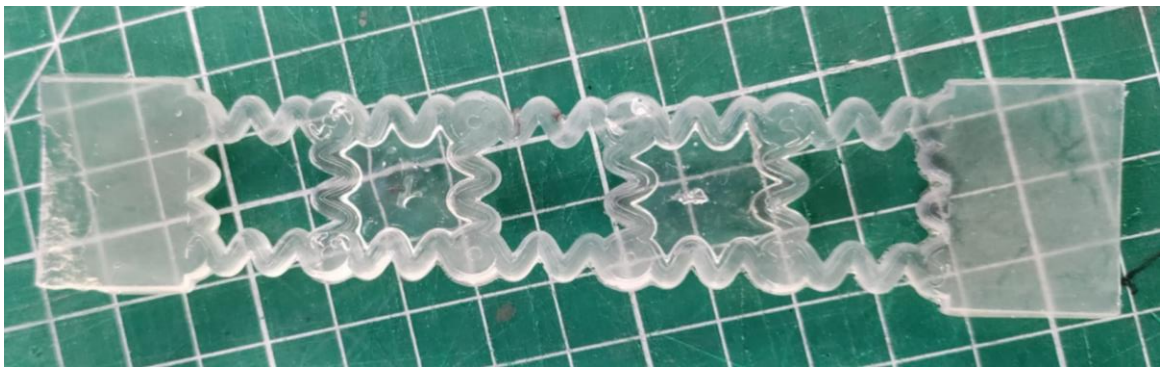

Figure 17. example of a test strip with several areas that are filled in by the 3D printer.

The number of tests that were performed for each variable was limited to three tests. Increasing the number of samples, would improve the accuracy for estimating E_a for each pattern.

During the fatigue test, the loading frequency was lower than the natural frequency of the heart. The loading frequency could not be higher due to the speed of the crosshead was limited by the machine. The use of a lower loading frequency could be considered a limitation. However, low loading frequencies does not affect the fatigue life of this fatigue test. Fatigue life is affected by crack initiation and crack propagation. At high load low cycle frequency, crack propagation dominates fatigue life [26]. As the high load can easily initiate a crack. For low load high frequency, crack initiation dominates fatigue life. Therefore, surface finish is important as locations where there is a defect in the surface finish, a crack can be more easily initiated [27]. The fatigue test in this study was a high load low frequency test since the sample had to be able to withstand the high deformations of the heart. A new experiment with a higher loading and unloading frequency could be performed to validate the results obtained in this study.

3D printing is a great technology for rapid prototyping of designs. However, depending on the model, post-processing was needed. For this model the structure of the sock was fragile and had to be supported by a significant amount of scaffolding. To be able to remove the scaffolding, the sock was stretched to its limits and in some occasions this resulted in breaking of the wave pattern. The broken wave pattern was manually repaired and after visual inspection it did not influence the properties of the sock. However, the stretching could have caused for crack initiation at different locations that were not visible. Therefore, a stronger pattern is needed that can be more easily deformed without failure and that needs less scaffolding.

Due to the weight of the electrode wires the electrode array needed to be held in place with the help of suture wires. The pulling of the wires caused the six electrodes to lose contact with the heart and could have caused for misalignment of the electrodes. However, this study was a feasibility test. In future experiments the design of the electrode array can be adjusted to prevent this from happening.

5.3. Future prospects

As the feasibility for a 3D printed electrode array was tested. Further development is needed for the electrode array to meet all the requirements that have been set in Section 2.1. The current sock elastically fit over the heart, however it had to be handled with care as it could easily break. To improve the ease of use for the sock, the durability needs to be increased. There are two methods for making the sock more durable. The first method is by rotating the wave pattern by 45˚ (Figure 18). During fatigue testing, it was noticed in some samples after the failure of two connections that were diagonally from each other (Figure 13), the samples would hinge around the broken interconnect. The hinging of the samples allows for facilitating higher strains at lower stress. By rotating the wave pattern 45˚, it is thought to reduce E_a of a pattern further. With a lower E_a there would be less failing of the connections between the electrodes, making the sock more durable.

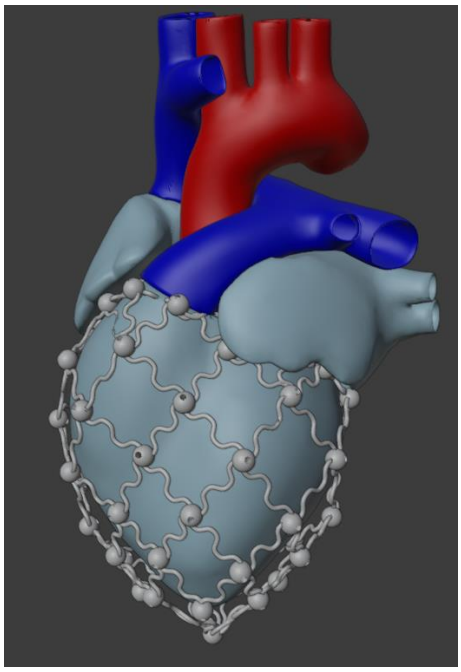

Figure 18. Example of a sock design with the pattern rotated by 45˚

The second method is by printing the sock on a 3D mold, overprinting [7]. By printing the sock over a mold, which can be later removed, it gives the opportunity to make use of different materials that cannot be used for standard 3D printing. These materials could be more tear-resistant and more elastic than the resin that was used for the current sock. Added benefits of using a mold to print on, is that the removal of scaffolding is easier, electronic wires and printed circuit boards could be integrated during printing.

To meet the requirement for high spatial resolution, a different approach is needed. Mapping studies at the Erasmus MC made use of a high-resolution flexible plaque electrode [30]. Small high-density electrode patches should be designed that attach to the sock at the position of current electrodes. The signal of the high-density patch electrodes should be processed by an application specific integrated circuit (ASIC). The power delivery and data transport is facilitated by an optical link, demonstrated in a study by Frank [12]. The optical link reduces the number of wires needed for receiving the electrode data, making it more practical to handle the electrode array, reduces the weight, and galvanic insulates the system [12]. By using light as a source for transmitting the electrode data, the signals will less influenced by noise from neighboring wires [25].

The final step to make the whole system usable is to correctly display the activation patterns on a virtual heart, where the recording positions have to be measured. To localize the electrodes on the heart, an interesting technique like Fiber Optical Shape Sensing (FOSS) could be used. This technology allows for high spatial resolution for determining the 3-dimensional shape of the optical fiber, and is not affected by environmental factors, like temperature and electrical fields [23]. FOSS works by sending laser light through a multi-core optical fiber (Figure 19A). The light is reflected back to the laser as each fiber has fiber Bragg gratings. By analyzing the receiving light, twists and bends of the multi-core optical fiber can be detected, and a 3D shape can be reconstructed [23, 28] (Figure 19B). When compared to EM tracking, FOSS is not sensitive to external disturbances and potentially has a higher accuracy [23]. By wrapping a FOSS fiber around the electrode array, covering all the intersections, the positions of the electrodes on the heart can be found by correlating the specific points of the optical fiber to each intersection. Consequently, a 3D shape of the electrode array can be created. As the sock is placed over the heart, the electrode positions are accurately recorded by

the system and the location data can be used to localize the electrodes on the heart. For these reasons, FOSS is an interesting technology allowing for localization of the electrode positions on the heart. This technology can also be used for the patch electrodes. The electrodes on the patch have a fixed distance from each other and the intersections. This fixed relationship between the intersections and the patch electrodes can be used to locate the electrode positions of the patch electrode on the epicardial surface. With this method, only the locations of the electrode locations need to be recorded to visualize the activation patterns of the heart.

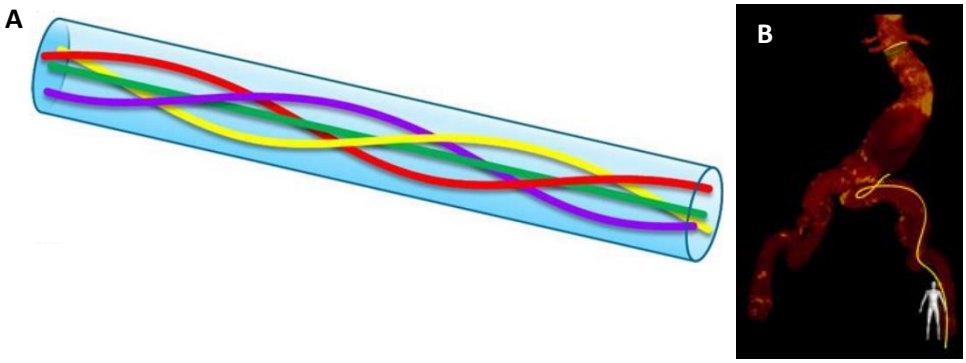

Figure 19. A. Visualization of the arrangement for the optic fibers in the multi-core fiber. Image taken from [22]. B. A 3D reconstruction of the FOSS fiber visualized over a computed tomography angiogram of the iliac artery. Image taken from [27].

In the future, the epicardial sock can be used for a wide variety of applications. For example for the help of the functional assessment of donation after circulatory death (DCD) hearts transported on machine perfusion. Recently, trials with hearts acquired from DCD have been successfully used for cardiac transplantation with use of isolated organ perfusion. With this success, the interest in using DCD hearts for transplantation was reawakened, as the DCD hearts could increase the availability of donor hearts. However, after the heart has been excised from the donor, the functional state of the heart is unknown since the time between cessation of life support and the excision of the donor heart (circulatory arrest and when the transplant operation can begin), varies significantly. During this time, the heart is deprived of oxygen (O_2) and nutrients. Cells will start to die causing myocardial ischemia and degrade the function of the heart for transplantation [21]. Currently, the only method for evaluating the function of DCD hearts is by visual inspection and lactate profiles [10]. However, lactate perfusion assessment and visual inspection is not a viable method for evaluating the DCD heart. The electrode array can be a supplementary method for the evaluation of DCD hearts.

6. Conclusion

This is the first study that has developed a 3D printed electrode array that can record the electrical activity of the ventricular surface at multiple sites simultaneously. A prototype electrode array was developed with 37 electrodes, a thickness of 1,5 mm, and modified sine wave design with amplitude of 0.5π and a length of 2 wavelengths. The electrode array was able to record the ventricular electrical activity and by correlating the anatomical landmarks to the electrode position, the activation pattern was displayed on a 3D model. This is the first step towards development of a biventricular electrode array for studies investigating cardiac arrhythmias. Further development is needed of the design to help elucidate the mysteries behind the activation patterns during arrhythmia's. To be able to use the electrode array in a clinical environment, further research is needed.

7. References

1. Amesz, J., et al., *Cardiac mapping on ex vivo perfused porcine slaughterhouse hearts: A Langendorff perfusion protocol for epicardial mapping on isolated beating hearts*, in *TU Delft Mechanical, Maritime and Materials Engineering; TU Delft Biomechanical Engineering*. 2020, Delft University of Technology.
2. Antzelevitch, C. and A. Burashnikov, *Overview of Basic Mechanisms of Cardiac Arrhythmia.* Card Electrophysiol Clin, 2011. **3**(1): p. 23-45.
3. Balser, J.R. and A. Thompson, *Chapter 40 - Cardiac electrophysiology*, in *Foundations of Anesthesia (Second Edition)*, H.C. Hemmings and P.M. Hopkins, Editors. 2006, Mosby: Edinburgh. p. 485-497.
4. Bear, L.R., et al., *Cardiac electrical dyssynchrony is accurately detected by noninvasive electrocardiographic imaging.* Heart Rhythm, 2018. **15**(7): p. 1058-1069.
5. Bhakta, D. and J.M. Miller, *Principles of electroanatomic mapping.* Indian Pacing Electrophysiol J, 2008. **8**(1): p. 32-50.
6. Bodson, L., K. Bouferrache, and A. Vieillard-Baron, *Cardiac tamponade.* Current Opinion in Critical Care, 2011. **17**(5).
7. Boros, R., P. Kannan Rajamani, and J.G. Kovacs, *Combination of 3D printing and injection molding: Overmolding and overprinting.* Express Polymer Letters, 2019.
8. Carlsson, M., et al., *Total heart volume variation throughout the cardiac cycle in humans.* American Journal of Physiology-Heart and Circulatory Physiology, 2004. **287**(1): p. H243-H250.
9. Carnero, B., et al., *Microfluidic devices manufacturing with a stereolithographic printer for biological applications.* Materials Science and Engineering: C, 2021. **129**: p. 112388.
10. Cernic, S., et al., *Lactate during ex-situ heart perfusion does not predict the requirement for mechanical circulatory support following donation after circulatory death (DCD) heart transplants.* The Journal of Heart and Lung Transplantation, 2022.
11. de Bakker, J.M., *Electrogram recording and analyzing techniques to optimize selection of target sites for ablation of cardiac arrhythmias.* Pacing and clinical electrophysiology : PACE, 2019. **42**(12): p. 1503-1516.
12. Frank, A., et al. *A 96-Channel Electrophysiology Catheter with Integrated Read-Out ASIC and Optical Link*. in *2021 43rd Annual International Conference of the IEEE Engineering in Medicine & Biology Society (EMBC)*. 2021.
13. Herakovich, C.T., *Thin-Walled Pressure Vessels*, in *A Concise Introduction to Elastic Solids: An Overview of the Mechanics of Elastic Materials and Structures*, C.T. Herakovich, Editor. 2017, Springer International Publishing: Cham. p. 77-81.
14. Herzberger, J., et al., *Polymer Design for 3D Printing Elastomers: Recent Advances in Structure, Properties, and Printing.* Progress in Polymer Science, 2019. **97**: p. 101144.
15. Hong, S., S. Lee, and D. Kim, *Materials and Design Strategies of Stretchable Electrodes for Electronic Skin and its Applications.* Proceedings of the IEEE, 2019. **107**(10): p. 2185-2197.
16. Josephson, M.E. and E. Anter, *Substrate Mapping for Ventricular Tachycardia: Assumptions and Misconceptions.* JACC: Clinical Electrophysiology, 2015. **1**(5): p. 341-352.
17. Kaplan, J., A. Kanwal, and V. Lala, *Reentrant Arrhythmias.* 2022.
18. Ladas, T.P., et al., *Fundamentals of Cardiac Mapping.* Cardiac Electrophysiology Clinics, 2019. **11**(3): p. 433-448.
19. Lampert, B.C., *Right Heart Catheterization*, in *Encyclopedia of Cardiovascular Research and Medicine*, R.S. Vasan and D.B. Sawyer, Editors. 2018, Elsevier: Oxford. p. 298-306.
20. Madadi, S., *Chapter 17 - Mechanisms, Diagnosis, and Therapy of Cardiac Arrhythmia*, in *Practical Cardiology (Second Edition)*, M. Maleki, A. Alizadehasl, and M. Haghjoo, Editors. 2022, Elsevier. p. 319-327.

21. Madan, S., et al., *Feasibility and Potential Impact of Heart Transplantation From Adult Donors After Circulatory Death.* Journal of the American College of Cardiology, 2022. **79**(2): p. 148-162.
22. Marieb, E.N. and K. Hoehn, *Human anatomy & physiology*. 2016, Pearson Education Limited: Harlow.
23. Megens, M., et al., *Shape accuracy of fiber optic sensing for medical devices characterized in bench experiments.* Med Phys, 2021. **48**(7): p. 3936-3947.
24. Mouws, E., et al., *Impact of Ischemic and Valvular Heart Disease on Atrial Excitation:A High-Resolution Epicardial Mapping Study.* J Am Heart Assoc, 2018. **7**(6).
25. Price, J. and T. Goble, *10 - Signals and noise*, in *Telecommunications Engineer's Reference Book*, F. Mazda, Editor. 1993, Butterworth-Heinemann. p. 10-1-10-15.
26. Qaiser, N., et al., *Design Criteria for Horseshoe and Spiral-Based Interconnects for Highly Stretchable Electronic Devices.* Advanced Functional Materials, 2021. **31**(7): p. 2007445.
27. Smith, C.B. and R.S. Mishra, *Chapter 4 - Case Study of Aluminum 5083-H116 Alloy*, in *Friction Stir Processing for Enhanced Low Temperature Formability*, C.B. Smith and R.S. Mishra, Editors. 2014, Butterworth-Heinemann: Boston. p. 19-124.
28. van Herwaarden, J.A., et al., *First in Human Clinical Feasibility Study of Endovascular Navigation with Fiber Optic RealShape (FORS) Technology.* European Journal of Vascular and Endovascular Surgery, 2021. **61**(2): p. 317-325.
29. Vanfleteren, J., et al., *Printed circuit board technology inspired stretchable circuits.* MRS Bulletin, 2012. **37**(3): p. 254-260.
30. Yaksh, A., et al., *A novel intra-operative, high-resolution atrial mapping approach.* J Interv Card Electrophysiol, 2015. **44**(3): p. 221-5.

Appendix

Appendix A Python code for modifying the blender model

Making the wave pattern

```
import bpy
import bmesh
import numpy as np


obj = bpy.context.edit_object
me = obj.data
bm = bmesh.from_edit_mesh(me)



###___Copy object___###
O_vertices = [i.index for i in bm.verts]
#O_faces = [0]
O_faces = [i.index for i in bm.faces]
O_edges = [i.index for i in bm.edges]
#for i in bm.faces:
#   O_faces.append(i)
#print('O_faces = ', O_edges)
edgedic ={}
e = []
for i in O_faces:
   #x = bm.faces[i].edges
   #x=bm.faces[i].index
   e = []
   for ii in bm.faces[i].edges:
      e.append(ii.index)
   edgedic.update({i:e})

vertdic = {}
e = []
for i in O_edges:
   #x = bm.faces[i].edges
   #x=bm.faces[i].index
   e = []
   for ii in bm.edges[i].verts:
      e.append(ii.index)
   vertdic.update({i:e})

###____Make waveform___###
number_of_cuts = 128
number_of_waves = 3
# Get x values of the sine wave
x1 = np.arange(0,((2*number_of_waves)*np.pi),(2*number_of_waves)*np.pi/(number_of_cuts))
```

```
# amplitude of the sine wave is sine of a variable like time
#y = 2*np.cos(x1)
#y = np.sign(np.cos(x1))*np.sqrt(np.abs(np.cos(x1)*4))
y = 0.5*np.pi*np.cbrt(np.sin(x1))
#y = 4*np.power(np.sin(x1),(1/3.72))
#y= 2*np.sin(x1)
#y = np.sqrt((1+2)/(1+2*(np.sin(x1)*np.sin(x1))))*np.sin(x1)*2
###___Get indices of the vertices___###
face_ind = [0]
#face_ind = [i.index for i in bm.faces]
verts_list_done = []
edges_completed = []
faces_completed = []
new_edges = []

for i in edgedic:
  print('Starting with face ', i)
  face_edges = edgedic[i] #[xx.index for xx in bm.faces[i].edges]

  #edge_verts = bm.faces[i].edges[||].verts
  edge_count = 0
  lengte_loop =  len(edgedic[i])
  #lengte_loop = len(face_edges)
#   print('loop length = ', lengte_loop)
#   print('edge count = ', edge_count)
#   print('face edges = ', face_edges)
  while edge_count < lengte_loop:
    print('loop length = ', lengte_loop)
    print('edge count = ', edge_count)
    print('current edge = ', face_edges[edge_count])
    bm.edges.ensure_lookup_table()
    current_edge = face_edges[edge_count]
    active_verts = vertdic[current_edge] #[bm.edges[current_edge].verts[0].index,
bm.edges[current_edge].verts[1].index]

    if current_edge not in edges_completed:
      #if active_verts[0].index  not in verts_list_done and active_verts[1].index not in
verts_list_done:            #check of de vertices al gebruikt zijn


   ###___subdivide edge___###
      #print('current egde = ', bm.edges[face_edges[edge_count]].index)
      face_edge = bm.edges[current_edge]
      print('subdividing face edge = ', face_edge)
      bpy.ops.mesh.select_all(action = 'DESELECT')
      bm.verts.ensure_lookup_table()
      bm.verts[active_verts[0]].select = True
      bm.verts[active_verts[1]].select  = True
      x = bmesh.ops.subdivide_edges(bm, edges=[face_edge], cuts=number_of_cuts)
      bmesh.update_edit_mesh(me)
```

```
####___Get vertices to of the other corneres of the planes___###

        #select neighbouring faces of the edge
        face1 = x['geom'][len(x['geom'])-2].index
        face2 = x['geom'][len(x['geom'])-1].index
        point_for_normal = []
        print('face1 = ', face1)
        print('face2 = ', face2)
        #print('starting face 1:')

#face 1
        if type(x['geom'][len(x['geom'])-2]) == bmesh.types.BMFace and type(x['geom'][len(x['geom'])-
1])== bmesh.types.BMFace:
            for j in edgedic[face1]:
              #print('number of edges are = ', j)
              if j in O_edges:
                 #print('edge of face 1 = ', j)
                 bm.edges.ensure_lookup_table()
                 for jj in vertdic[j]:
                    vert = jj
                    bm.verts.ensure_lookup_table()
                    d = len(bm.verts[vert].link_edges)
                   # print('vert of edge  = ', vert)
                    if d > 4:
                      if vert in O_vertices and vert not in point_for_normal:
                         point_for_normal.append(vert)
                        # print('vertex at top (d) = ', d)
                    if d < 5:
                      if vert in O_vertices and vert not in active_verts and vert not in point_for_normal:
                          point_for_normal.append(vert)
                          # print('d = ', d)
                          # print('vertice of face = ', vert)

    ##              bm.edges.ensure_lookup_table()
    ##              bm.edges[j.index].verts[0].index
    ##              bm.edges[j.index].verts[1].index
    ##              if bm.edges[j.index].verts[0].index in O_vertices and bm.edges[j.index].verts[1].index
in O_vertices and bm.edges[j.index].verts[0].index not in active_verts and
bm.edges[j.index].verts[1].index not in active_verts:
    ##                  point_for_normal.append(bm.edges[j.index].verts[0].index)
    ##                  point_for_normal.append(bm.edges[j.index].verts[1].index)
            #print('point_for_normal = ', point_for_normal)
            #print('active points = ',active_verts[0],active_verts[1])
    #         print('starting face 2:')
```

```
  ##face 2
        for j in edgedic[face2]:
          #print('number of edges are = ', j)
          if j in O_edges:
            #print('edge of face 2 = ', j)
            bm.edges.ensure_lookup_table()
            for jj in vertdic[j]:
              vert = jj
              bm.verts.ensure_lookup_table()
              d = len(bm.verts[vert].link_edges)
              #print('vert of edge  = ', vert)
              if d > 4:
                if vert in O_vertices and vert not in point_for_normal:
                  point_for_normal.append(vert)
                  #print('vertex at top (d) = ', d)
              if d < 5:
                if vert in O_vertices and vert not in active_verts and vert not in point_for_normal:
                  point_for_normal.append(vert)
                  #print('d = ', d)
                  #print('vertice of face = ', vert)
  #       bmesh.update_edit_mesh(me)
        print('point_for_normal = ', point_for_normal)
        print('active points = ',active_verts[0],active_verts[1])
        normal = np.cross((obj.matrix_world@bm.verts[point_for_normal[0]].co-
obj.matrix_world@bm.verts[point_for_normal[1]].co),
(obj.matrix_world@bm.verts[point_for_normal[0]].co-
obj.matrix_world@bm.verts[point_for_normal[2]].co))
      else:
        normal = bm.faces[i].normal


####___Calculate normal of a plane___###
      print('calculating normal')
      print('active points = ',active_verts[0],active_verts[1])
#       bm.verts.ensure_lookup_table()
#       print('A = ', bm.verts[point_for_normal[0]].index)
#       print('B = ', bm.verts[point_for_normal[1]].index)
#       print('C = ', bm.verts[point_for_normal[2]].index)
      #normal = np.cross((obj.matrix_world@bm.verts[point_for_normal[0]].co-
obj.matrix_world@bm.verts[point_for_normal[1]].co),
(obj.matrix_world@bm.verts[point_for_normal[0]].co-
obj.matrix_world@bm.verts[point_for_normal[2]].co))
      bm.verts.ensure_lookup_table()
      BA= obj.matrix_world@bm.verts[active_verts[0]].co-
obj.matrix_world@bm.verts[active_verts[1]].co
      Bb = np.cross(normal, BA)
      Bb_scale = np.sqrt((Bb[0]*Bb[0])+(Bb[1]*Bb[1])+(Bb[2]*Bb[2]))
      Bb_norm = Bb/Bb_scale
#       print('normaal = ', normal)
#       print('BA = ', BA)
#       print('Bb = ', Bb)
#       print('Bb_scale = ', Bb_scale)
```

```
        print('Bb_norm = ', Bb_norm)
        replace_edge = []
        #bpy.ops.mesh.select_all(action = 'DESELECT')
        for e in x['geom_inner']:
          e.select = True

          replace_edge.append(e.index)
        print('replace edge = ', replace_edge)


        unit_vector_1 = bm.faces[i].normal / np.linalg.norm(bm.faces[i].normal)

        unit_vector_2 = normal/ np.linalg.norm(normal)

        dot_product = np.dot(unit_vector_1, unit_vector_2)

        angle = np.arccos(dot_product)
        hoek = angle*180/np.pi
        print('angle = ', angle*180/np.pi)

    ###___Move points___###
    #if (current_edge%2) ==0
        #if angle <1.57079633:
       # if  i >= 0 :#(active_verts[1]-active_verts[0]) >0: #*(active_verts[0]-active_verts[1]) < 2 and
angle <1.57079633:
        if hoek >90:# and (current_edge%2) ==0:
           print('moving points')
           for v in replace_edge:
             vv = replace_edge.index(v)
                           # deselect all first

             #select vertex
             bm.verts[v].select = True
#              bmesh.update_edit_mesh(me)

             scale = np.sqrt((BA[0]*BA[0])+(BA[1]*BA[1])+(BA[2]*BA[2]))/128
             print('point = ', vv)
             print('y = ', y[vv])
             print('scale = ', scale)


             movement = y[vv]#*scale                  #determines how much the vertex is moved
             invert = obj.matrix_world.inverted()
             global_co = obj.matrix_world@bm.verts[v].co
             global_co[0] = global_co[0]+(Bb_norm[0]*movement)
             global_co[1] = global_co[1]+(Bb_norm[1]*movement)
             global_co[2] = global_co[2]+(Bb_norm[2]*movement)
             local_co = invert@global_co
```

```
            bm.verts[v].co = local_co
#               bpy.ops.transform.translate(value=(Bb_norm[0]*movement,Bb_norm[1]*movement,
Bb_norm[2]*movement), orient_type='GLOBAL', orient_matrix=((1, 0, 0), (0, 1, 0), (0, 0, 1)),
orient_matrix_type='GLOBAL', mirror=True, use_proportional_edit=False,
proportional_edit_falloff='SMOOTH', proportional_size=1, use_proportional_connected=False,
use_proportional_projected=False)

#               bpy.ops.transform.translate(value=(Bb_norm[0]*movement,Bb_norm[1]*movement,
Bb_norm[2]*movement), orient_type='GLOBAL')          #Bb_norm is the normalized vector
            bm.verts[v].select = False
#               bmesh.update_edit_mesh(me)
            print('movement = ', movement)
            print('translate value = ', Bb_norm[0]*movement,Bb_norm[1]*movement,
Bb_norm[2]*movement)

            #print(vv,v, movement)
   #        print('movement = ', movement)
   #        print('scale = ', scale)
   #        print('displacement = ', (Bb_norm[0]*movement,Bb_norm[1]*movement,
Bb_norm[2]*movement))
          bmesh.update_edit_mesh(me)
          print('uneven')

          verts_list_done.append(active_verts[0])
          verts_list_done.append(active_verts[1])
          edges_completed.append(current_edge)
          print('completed edges = ',edges_completed)
          print('one edge completed')
        else:
          for v in replace_edge:
            vv = replace_edge.index(v)
                # deselect all first
            #select vertex
            bm.verts[v].select = True


            scale = np.sqrt((BA[0]*BA[0])+(BA[1]*BA[1])+(BA[2]*BA[2]))/128
            print('point = ', vv)
            print('y = ', -y[vv])
            print('scale = ', scale)


            movement = -y[vv]#*scale                  #determines how much the vertex is moved
            global_co = obj.matrix_world@bm.verts[v].co
            global_co[0] = global_co[0]+(Bb_norm[0]*movement)
            global_co[1] = global_co[1]+(Bb_norm[1]*movement)
            global_co[2] = global_co[2]+(Bb_norm[2]*movement)
            invert = obj.matrix_world.inverted()
            local_co = invert@global_co
```

```
            bm.verts[v].co = local_co
#               bm.verts[v].co.y = bm.verts[v].co.y+(Bb_norm[1]*movement)
#               bm.verts[v].co.z = bm.verts[v].co.z+(Bb_norm[2]*movement)
#               bpy.ops.transform.translate(value=(Bb_norm[0]*movement,Bb_norm[1]*movement,
Bb_norm[2]*movement), orient_type='GLOBAL', orient_matrix=((1, 0, 0), (0, 1, 0), (0, 0, 1)),
orient_matrix_type='GLOBAL', mirror=True, use_proportional_edit=False,
proportional_edit_falloff='SMOOTH', proportional_size=1, use_proportional_connected=False,
use_proportional_projected=False)

#               bpy.ops.transform.translate(value=(Bb_norm[0]*movement,Bb_norm[1]*movement,
Bb_norm[2]*movement), orient_type='GLOBAL')          #Bb_norm is the normalized vector
            bm.verts[v].select = False

            print('movement = ', movement)
            print('translate value = ', Bb_norm[0]*movement,Bb_norm[1]*movement,
Bb_norm[2]*movement)
      #         print('movement = ', movement)
      #         print('scale = ', scale)
      #         print('displacement = ', (Bb_norm[0]*movement,Bb_norm[1]*movement,
Bb_norm[2]*movement))
          bmesh.update_edit_mesh(me)

          verts_list_done.append(active_verts[0])
          verts_list_done.append(active_verts[1])
          edges_completed.append(current_edge)
          print('completed edges = ',edges_completed)
          print('one edge completed')
#
        edge_count = edge_count+1
     #edge_count = edge_count+1
#
     else:
        edge_count = edge_count+1

  faces_completed.append(i)
  print('going to next face')
#
print('lengt edges completed =', len(edges_completed))
print('done')
```

Adding the spheres

```
import bpy
import bmesh
import numpy as np


obj = bpy.context.edit_object
me = obj.data
bm = bmesh.from_edit_mesh(me)
radius = 5 # in mm
bpy.ops.object.vertex_group_select()
vert_index = []
for v in bm.verts:
    if v.select:
        print(v.index)
        vert_index.append(v.index)

bpy.ops.object.vertex_group_deselect()

for i in vert_index:
    bm.verts[i].select = True
    x = obj.matrix_world@bm.verts[i].co
    bmesh.update_edit_mesh(me)
    #bpy.ops.view3D.snap_cursor_to_selected()

    bpy.ops.mesh.primitive_uv_sphere_add(radius = radius, enter_editmode=False, align='WORLD',
location=(x[0], x[1], x[2]), scale=(1, 1, 1))
    bm.verts.ensure_lookup_table()
    bm.verts[i].select = False
    bmesh.update_edit_mesh(me)
    print('sphere added at =', i)

print('done')
```

Appendix B Fatigue test results

Sample		Cycle until failure
Pattern 1		
1,5 mm		
	Sample 1	352
	Sample 2	500
	Sample 3	1000
2,0 mm		
	Sample 4	507
	Sample 5	437
	Sample 6	176
2,5 mm		
	Sample 7	236
	Sample 8	79
	Sample 9	104
3,0 mm		
	Sample 10	74
	Sample 11	48
	Sample 12	36
Pattern 2		
1,5 mm		
	Sample 13	899
	Sample 14	1000
	Sample 15	1000
2,0 mm		
	Sample 16	209
	Sample 17	69
	Sample 18	366
2,5 mm		
	Sample 19	75
	Sample 20	123
	Sample 21	68
3,0 mm		
	Sample 22	74
	Sample 23	110
	Sample 24	74
Pattern 3		
1,5 mm		
	Sample 25	398
	Sample 26	689
	Sample 27	492
2,0 mm		
	Sample 28	377
	Sample 29	345
	Sample 30	427
2,5 mm		
	Sample 31	184
	Sample 32	292

3,0 mm		
	Sample 33	331
	Sample 34	139
	Sample 35	319

Appendix C Literature review

Recording the total electrical activity of the epicardial wall: a systematic overview.

Abstract

Cardiac electrophysiology is a medical field that is important for the identification of heart arrhythmias. Studying electrical activation patterns of the heart is gaining importance and has already led to new discoveries in the area of cardiac arrhythmias. The techniques used in these studies all have unique solutions for the problems that arise when recording electrical activity of the heart.

This systematic review gives an overview and compares the systems that have been used for measuring the total electrical activity of the heart. This review focuses on (1) how the electrical activity can be recorded, and (2) what methods can be used to locate the recording positions. Papers in PubMed and the Institute of Electrical and Electronics Engineers (IEEE) were investigated. The best method to record electrical activity of the heart is with unipolar electrodes. Localizing the position of the electrodes on the heart still remains a difficult task. To do this, a novel method needs to be developed that can measure the inter electrode distance (IED) simultaneously with the unipolar recordings of the epicardial surface. Measuring cardiac electrophysiology with several electrodes simultaneously, combined with a system for correct localization is possible, and would allow for a better understanding of the etiology of cardiac arrhythmias.

Introduction

Cardiac electrophysiology (EP) is important in the identification of heart rhythm diseases. By studying the electrical activity patterns of the heart, the causes of arrhythmias and how sinus rhythm (SR) is affected by heart diseases may be discovered [18, 29].

To gain new insight in how heart rhythm and cardiac functions are influenced by diseases and therapies, experiments are necessary [17]. However, experimentation on the human heart is not always possible, so an alternative has to be used. Therefore, experiments are usually performed on animals since these are readily available. When using pigs, the benefit they have is that they have similar characteristics to human hearts. *In vivo* animal models can give an accurate representation of the effects of a therapy in a complex system, but may bring risks to the animal. Animal models need to be ethical approved. Fortunately, ethical approval can be avoided when using *ex vivo* experiments as organ collection does not require ethical approval [21]. The Langendorff setup has become the golden standard for *ex vivo* heart perfusion (EVHP) experiments, as it provides a powerful platform for cardiovascular research [23]. The EP and functions can be compared between healthy and unhealthy hearts, and the effects of treatments can be studied on a stable isolated platform in the absence of autonomic influences [12, 23].

For the investigation of the EP parameters of the heart, tools are developed to measure the electrical potentials. One of these tools is cardiac mapping. Cardiac mapping is a method to systematically record epicardial potentials from the surface of the heart, which later can be spatially visualized [29]. As technology is developing, new tools are created to visualize and record epicardial potentials better. Higher spatial resolution cardiac maps can be made with electrode-arrays. To create high spatial resolution total cardiac maps, currently the EP measurements are obtained over multiple heart beats measured at different locations on the atria and ventricles. The maps are combined to display whole tissue activation after the experiment [2, 30]. High-resolution simultaneous multi-site mapping is currently not possible as technology is not yet developed sufficiently [30]. As cardiac EP characteristics can differ from beat-to-beat, simultaneous multi-site mapping has advantages over reconstructing conduction maps from multiple heart beats. Therefore, a system is needed that can record the electrical activation of multiples site on the cardiac surface at the same time.

The goal of this review is to give an overview of the systems that are being used for measuring the total electrical activation of the heart, give a comparison on the advantages and disadvantages of

each method, and come to a recommendation for developing a new epicardial mapping tool. Different groups each have developed their own method for recording the electrical activation. These methods bring their own challenges for measuring and interpreting electrical activation. The focus in this review will be on techniques that can be used in EVPH experiments .
The questions that are addressed are: (1) how is the electrical activation recorded, and (2) what method is used to locate the recording positions.

Methods

For this systematic review, a literature search was done in PubMed and the Institute of Electrical and Electronics Engineers (IEEE). The data was collected between 1st of November and the 15th of November 2021. The search term used to find the relevant articles was:
(epicardial AND (sock OR mesh)) AND electrode.
To determine which articles should be included in the review, they were scanned by title, abstract, and method. Articles which described a method to record electrical epicardial activation, or how the geometry of the heart is measured for recording the epicardial potentials were included in the study. From the included papers, the references were also inspected for additional relevant articles. If the method for signal recording was described in more detail in a previous paper from the same group, that paper was included instead of the paper from the search term.
Papers were excluded from the study if an epicardial sock was used, but there was no further information provided about how the sock was constructed, a similar study has already been done, does not provide information about the measuring method, or papers were not in English.

Results

The search yielded a total of 127 results. After removing duplicates, a total of 125 papers remained eligible for screening. Five papers were found additionally in the references of the 125 eligible papers. A total of 38 papers have been assessed by reading the full text. Of these papers, only 19 met the inclusion criteria (Figure 1) (Table 1). A total of 19 paper were excluded after full text assessment, of which 5 papers used work that had been done in a previous study by the same group, 3 papers were excluded because they were not available in English, and 11 papers didn't provide information about the measuring method. A total of 19 papers were obtained to be analyzed in detail.
Recording the activation location can be divided into 2 parts. Recording the potentials of the epicardium and locating the recorded signal on the heart. The first section of the results gives an overview of the different approaches that were taken for measuring the electrical activation of the epicardial surface. The second part focuses on methods used to locate the recorded signal on the epicardial surface.

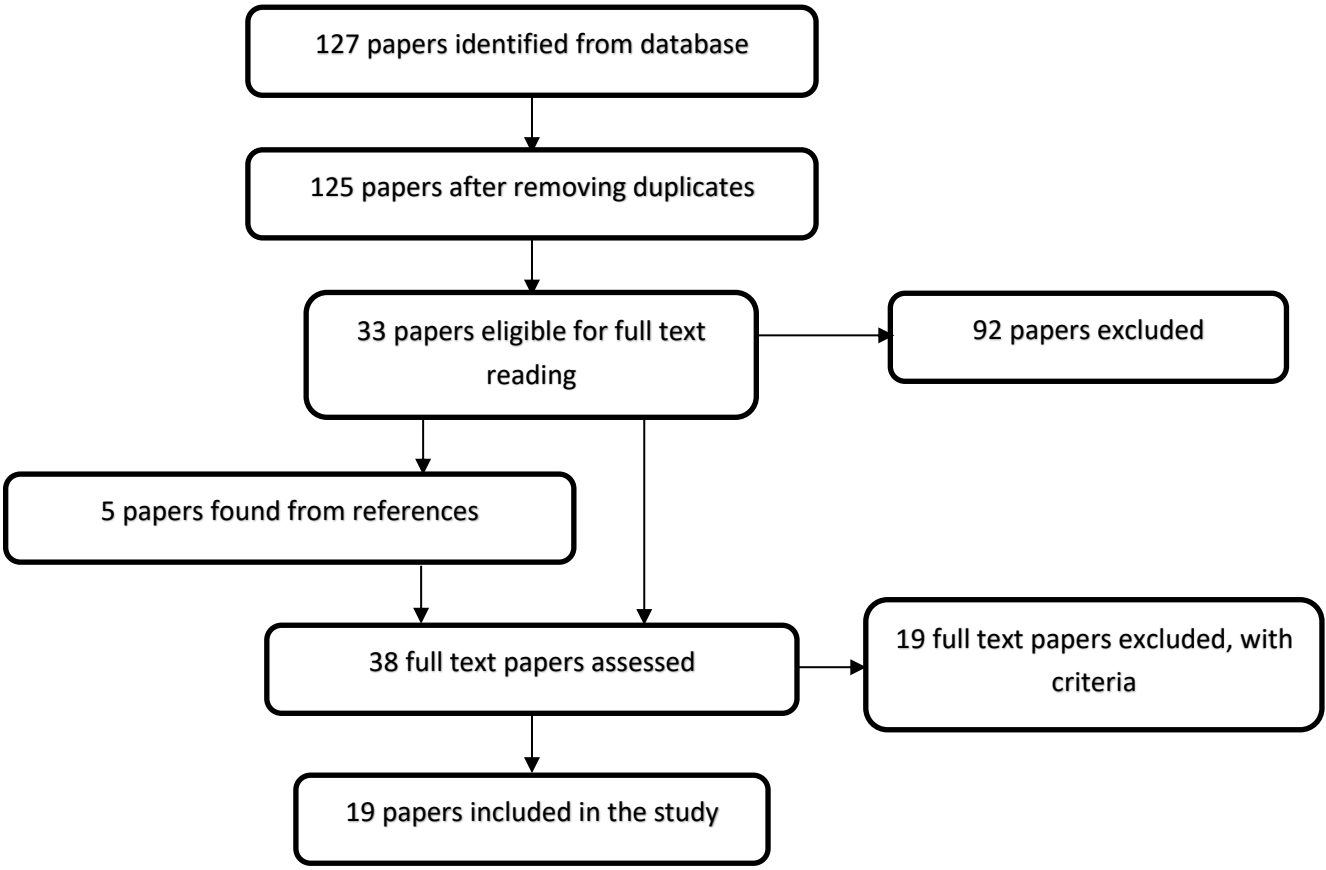

Figure 1. Modified PRISMA literature flow diagram

Table 1. Overview of the methods for recording electrical activation, locating electrodes, and specifications of the equipment used for recording electrical signals.

Authors	Recording method	Location positioning	Material	Inter electrode distance	Polarity
(Arisi et al., 1983)	1124 electrodes	Mesh	Nylon sock and silver electrodes	2 mm	Unipolar
(Bear et al., 2019)	108 electrodes and voltage sensitive dye (Di-4-ANBDQBS (10 µM))	3D fluoroscopy and optical map	No data	No data	Unipolar
(Brodine, Baker, Kirchmer, & Chiarelli, 1990)	10 electrodes	Mesh	Elastic band, gold plated electrodes	1.5 cm	Bipolar
(Chattipakorn et al., 1998)	504 electrodes	Mesh	Elastic sock and silver/ silver chloride electrodes	4 mm	Unipolar
(d'Alché, Clauser, Morel, & Gauthier, 1991)	240 electrodes	Mesh	Chloride silver electrodes, elastomer mesh	No data	Unipolar
(Dhein, Müller, & Klaus, 1990)	256 electrodes	Mesh	Silver electrodes	1 mm	Unipolar
(Downar et al., 1984)	110 electrodes	Mesh	Nylon sock, brass pins and Teflon discs	No data	Unipolar
(Faris et al., 2003)	126 electrodes	Surface to surface map from MRI and digitizer	Nylon mesh, copper electrodes	No data	Unipolar
(Harrison et al., 1980)	52 electrodes	Mesh	Nylon mesh, brass electrodes	2.5 mm	Unipolar and bipolar
Kay, Amison, & Rogers, 2004)	di-4-ANEPPS (10 µM)	Optical map	No data	No data	No data
(Kubota et al., 1993)	60 electrodes	Mesh	Silver electrodes	No data	unipolar
(Lavier, Meunier, & Savard, 1993)	No data	Mesh	No data	No data	No data

(Massé, Sevaptsidis, Parson, & Downar, 1991)	336 electrodes	CT scan	No data	No data	Unipolar
(Nash, Bradley, Kardos, Pullan, & Paterson, 2002)	127 electrodes	Echocardiography, predetermined shape, and digitizer arm	Stainless steel electrodes	7 mm	Unipolar
(Qu, Ripplinger, Nikolski, Grimm, & Efimov, 2007)	Voltage sensitive dye (di-4-ANEPPS (10µL/min)	3D geometry reconstruction	No data	No data	No data
(Taccardi et al., 1992)	630 electrodes	Digitized by protractor	Nylon stocking and silver electrodes	4 mm	Unipolar
(Wang, Yang, & Yu, 2014)	128 electrodes	Ct imaging and 3D model reconstruction	No data	3.5 mm	No data
(Wit et al., 1982)	192 electrodes	Mesh	Silver ball electrodes	4 mm	Unipolar and bipolar
(Worley et al., 1987)	60 electrodes	Mesh	Xspan™, epoxy, tin plated copper electrodes, stainless steel wire	No data	Bipolar

Electrical activity

The electrical activity can be measured in two different ways, by using voltage sensitive dyes (VSDs) or by using electrodes.

Dyes

VSDs allow for the visualization of changes in the membrane potential of tissue in real time with high temporal and spatial resolution. Tissues are stained by coronary perfusion as it delivers the dyes to the epicardial tissue [3, 13, 20]. By illuminating the VSD with its excitation wavelength, the dye fluoresces, which can be recorded by a charge coupled device (CCD) camera. A change in electrical activity will result in a change in intensity of fluorescence, which gives an indication of the activation [20]. When measuring electrical activation with VSDs motion artifacts play an important role in the accuracy of the recording. Therefore, the contraction is uncoupled from the activation by using 2, 3-butanedione monoxime (BDM) [9, 13, 20] or blebbistatin [3] by inhibiting ATPase activity.

Electrodes

The most used method to record the electrical activity of the heart, is with electrodes (Table 1). To secure the electrode array, different methods are used: an elastic sock that is fitted over the heart onto which the electrodes are mounted [2, 3, 4, 5, 6, 8, 10, 11, 14, 16, 19, 24, 27, 28]. The electrodes are fixed on the sock in different patterns. This will be further discussed in the second part of this study. Instead of using a sock, electrode arrays with a fixed inter electrode distance can be used so that the electrodes can be easier located on the epicardial wall [7, 25, 27]. The electrode arrays can be attached in an elastic manner to reduce the risk of damaging the epicardial tissue (Figure 2B) [7]. Another method to secure multiple flexible fixed electrode arrays to the atrium and pulmonary veins are sutures, as a sock has difficulties conforming to the shape of the atrium [25]. If the epicardial mapping is done for a short period of time, a hand-held plaque electrode is sometimes used for recording [27]. When placing an electrode array on the epicardial surface, if an electrode makes no or a poor contact to the epicardial surface, electrical activation can't be recorded [27].
Different materials were used for the electrodes (Table 1). To reduce the risk of corrosion and increase conductivity most electrodes were made from noble metals, mainly silver and gold [2, 4, 5, 6, 7, 14, 24, 27]. Copper was also used as it is affordable, readily available, and is MRI compatible [10, 28]. Other studies used brass and solder as electrode materials because they are inexpensive metals [8,11]. One paper used stainless steel for the electrodes as it is a common material in the medical field and known for its corrosion resistance [19].
For recording the electrical activation, two different types of recordings can be made; bipolar or unipolar recordings. Most studies used unipolar recording for their mapping protocol [2, 3, 5, 6, 7, 8, 10, 11, 14, 16, 19, 24, 27]. Unipolar recordings are bipolar recordings in essence, as two electrode leads are connected to the amplifier and the potential difference between the leads is measured. One of the electrode leads is attached somewhere on the body, this is the indifferent electrode. The other leads are placed on the area of interest, the exploring electrode. Bipolar electrodes don't use an indifferent electrode, and the electrode leads are placed close to each other. The voltage difference between the leads is amplified and recorded. The inter electrode distance for the bipolar recordings are 1 and 2 mm [4, 11, 27, 28]. A distance smaller than that does not gain any benefits for signal recording.

To record the changes in the voltages at the electrodes, the signal from each electrode lead must be saved. To convert the analog signal of the electrodes into digital signals, all measurements are simultaneously band pass filtered at 0.5 Hz and 500 Hz [4, 5, 6]. The filtered signal is then sampled at 1000 Hz [2, 6, 10, 15, 24] or 2000 Hz [3, 5,19]. This is saved on a local disc, on a pc or a tape to be reviewed later.
If the equipment cannot digitize all the electrode simultaneously the electrograms can be recorded over multiple heart beats at different locations. One electrode must be continuously recorded to be used as a time reference to later join all the data [2].

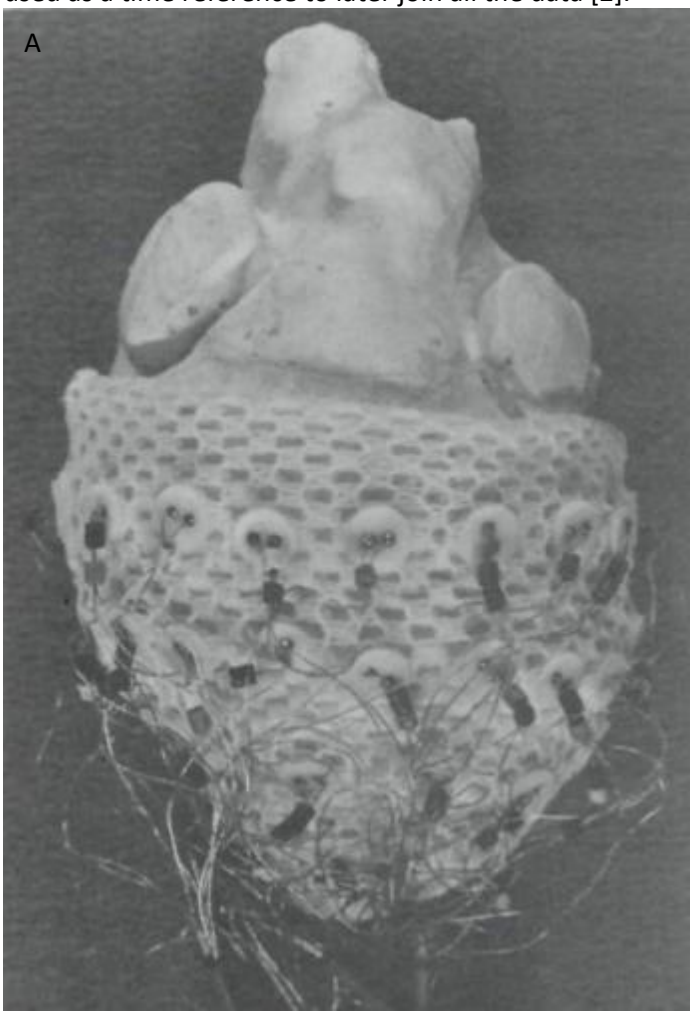

Figure 2. A. Sock electrode array. (Image taken from [11]). B. Experimental setup with plaque electrodes (Image taken from [7]).

Activation localization

Recording the electrical activation of the epicardial tissue is one part of the problem. To properly interpret the whole epicardial activity the position of the recorded signal must be known or estimated. This section discusses the different methods used to correlate the epicardial recordings to the correct anatomical position on the heart.

Mesh

The most common way to localize the electrodes is to make use of an electrode mesh on which the electrodes are placed in a regular interval or pattern. This mesh is then placed over the object and adapted to its shape [2, 4, 5, 6, 7, 8, 11, 14, 27, 28]. To orient the mesh in the correct way anatomical landmarks are used to align the mesh with the heart (Figure 3) [4, 5, 8, 11, 15]. A cheap and compliant material that was chosen as base material onto which the electrodes can be mounted is nylon [2, 8, 10, 11, 24]. Xspan™ was developed by one group as the nylon mesh was not compliant enough, and the electrodes failed regularly [28]. The pattern in which the electrodes are mounted onto the mesh was used for the visualization of the activation patterns of the heart.

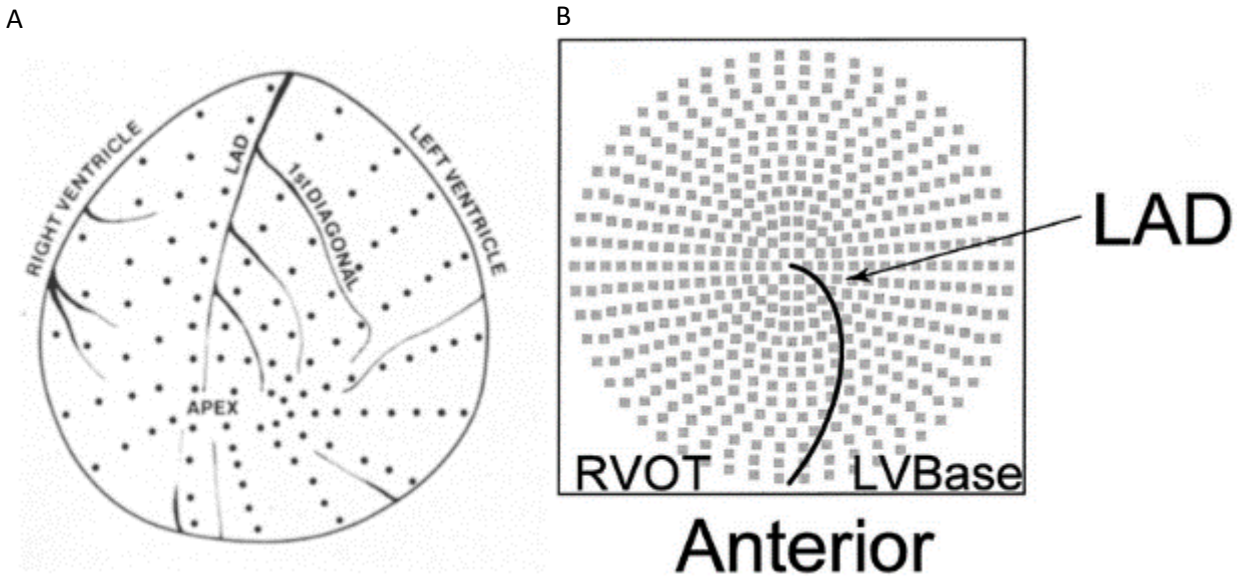

Figure 3 A. Polar projection of the electrode pattern lay-out with the apex at the center (image taken from [8]), B. Projection of the electrode sock seen from the apex which was used for the display of electrical activation (Image taken from [5]).

Computed tomography

Computed tomography (CT) uses X-rays to reconstruct a 3D image of the object. The heart can be later segmented using an algorithm, enabling visualization of the cardiac activation patterns. The acquired CT images can be segmented and using a reconstruction algorithm, the 3D surface model is generated [15, 25]. The visualization of the electrodes on the model is obtained by manually selecting the position of two electrodes. As the electrodes in the array are spaced in a regular pattern, the positions of the whole electrode array can be calculated using an interpolation algorithm and projected on the model surface [15, 16, 25]. Another use of the CT images is to precisely measure the location of the electrodes on the heart [3, 16]. The electrode locations can be used to create a model to display activation patterns [16], or to align a virtual camera for 2D optical recordings [3].

Magnetic resonance imaging

A method that exposes the patient to less radiation is magnetic resonance imaging (MRI). It is a non-invasive imaging technique that makes use of magnetic fields and radio frequency (RF) pulses to visualize structures inside the human body. To visualize the epicardial sock in MRI images, small glass beads filled with 18 µL of gadolinium-diethylenetriamine pentaacetic acid (Gd-DTPA) (~ 5 mM) are attached at specific locations on the sock. Since Gd-DTPA is an MRI contrast agent, the glass beats are clearly visible on the images [10]. By recording the electrode locations and the glass beads with a digitizer arm, the electrode locations of the sock were transformed onto the model acquired from the MRI images [10].

Ultrasound

An alternative for imaging inside the patient, is ultrasound [19]. Ultrasound uses high frequency sound waves to create images of structures in the human body. Ultrasound is known for its use in making images of fetuses in the womb. Visualization by ultrasound can be improved by mounting an ultrasound probe onto a digitizer arm, enabling visualization of the 3D geometry of soft tissues, like the heart [19]. With the geometry of the heart obtained, the electrode locations can be projected onto the model (Figure 4) [19].

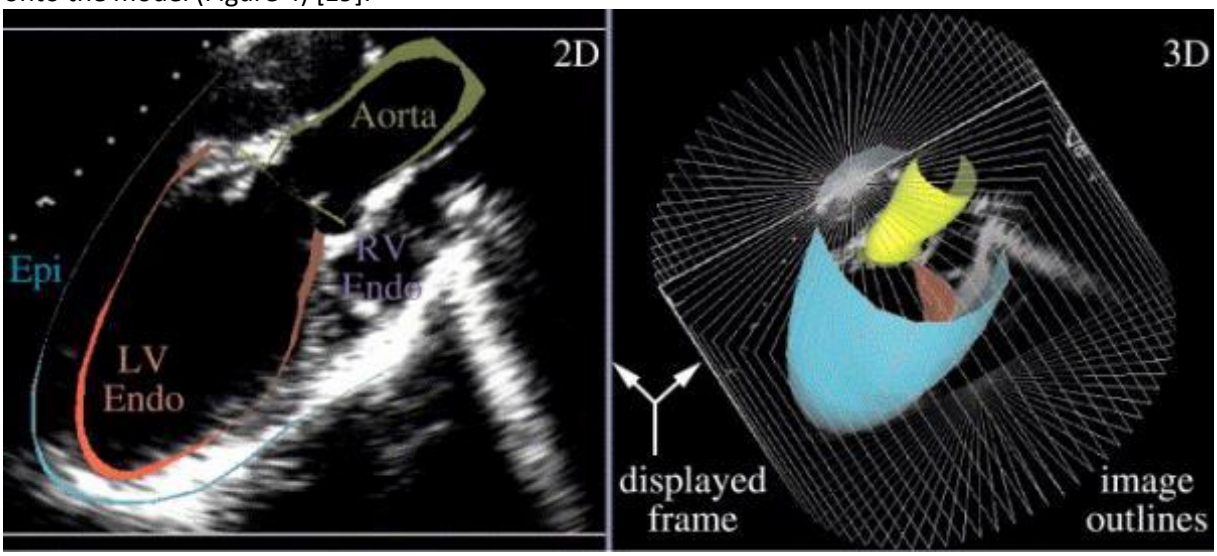

Figure 4. On the left panel the image captured by the ultrasound probe that was used to construct the 3D model with segmented surfaces, epicardial (Epi), Left ventricle endocardial (LV Endo), and Right ventricle endocardial (RV Endo). On the right panel the reconstructed 3D ventricular model. (Image taken from [19])

Digitizer arm

Previous methods for localizing the electrodes on the heart were supplemented by using data from a digitizer arm and then transforming the electrode coordinates of the digitizer arm into a geometry model [10, 19]. A digitizer arm is an electromechanical device that can be moved by the user (Figure 5). The position of the tip of the digitizer can be accurately calculated from the angles of the joints of the arm. A 3D model can be generated from the point cloud data of the electrodes [24]. This model was then be used to display the epicardial activity at the correct locations.

Figure 5. 3D digitizer arm used in [10]

Optical

Optical methods are mainly used in *ex vivo* experiments. The heart must be positioned in front of a camera and high-resolution images are taken from multiple angles [13, 20]. An algorithm segments the contours of the heart from the image, and by subtracting the contours at different angles, from a 3D cube a surface model is calculated [13,20]. The optical method is chosen for its high spatial resolution compared to the previously discussed techniques. When generating the 3D model by projecting the surface images onto the model, the epicardial activity can be easily visualized.

Discussion

A systematic review was conducted to investigate the different recording systems that are being used for measuring total electrical activity of the epicardial tissue and compare the different methods to each other.

Electrical activity

There are two main methods for measuring electrical activation of the heart: optically or with the use of electrodes. The main advantage of recording the activation pattern optically is a high spatial resolution. When recording a beating heart, camera motion artifacts occur due to the contraction of the muscles. This plays a role in the accuracy of the measurement [3, 13]. Motion artifacts can be solved by using BDM or blebbistatin that prevents contraction of the heart muscle fibers. The agent itself can have an influence on the conductivity of the heart tissue, but this is usually neglected. Furthermore, VSD's have a low signal to noise ratio (SNR) due to the fluorescence of the tissue itself. In addition, over-exposing the tissue with too much light will photo bleach the dye, reducing the signal [3, 13]. Finally, when recording the signals optically only the visible area can be measured. As the heart is a 3D shape, parts of the epicardial tissue will be obscured by the geometry itself. Using a panoramic setup increases the visible area of the heart surface as well as the complexity of the system [13].

With electrodes, the activation pattern can be measured in a unipolar or bipolar configuration. From unipolar signals the direction of the wave propagation can be observed. Unipolar electrode recordings are affected by far field effects that are caused by distant electrical activation. This can be reduced by filtering. However, filtering will reduce the information available in the signal. Bipolar electrodes are not influenced by far field effect. This is due to the close proximity of both electrodes. Both electrodes record similar distant activity. When calculating the difference between the electrodes the far field effects are canceled out. Due to this, only local information is measured, and the direction of wave propagation is lost. Also, if the wave propagates perpendicular to the electrode pair, due to how bipolar signals are measured, activation will not be recorded. The limitation of loss of information can be solved by using an array of bipolar electrodes. By visualizing the activation pattern, the direction how the wave is propagating can be determined. With unipolar electrodes in an array, it is possible to calculate the bipolar electrogram from the unipolar electrograms. It is not possible to calculate the unipolar recordings from the bipolar recordings due to the lack of an indifferent electrode. If a bipolar array would use an indifferent electrode, it would be possible to calculate the unipolar signals. Therefore, most studies in this literature review made use of unipolar electrode arrays (Table 1).

A signal can only be measured when the electrodes make good contact with the tissue. This is accomplished by using an elastic mesh, sutures, or an array. Most studies use an elastic mesh that will conform to the shape of the heart. However, as the heart contracts during one beat some areas will lose contact with the epicardial wall as the fit of the sock is never perfect. This will prevent the recording of the electrogram [27, 28]. To secure the electrode mesh more tightly to the epicardial wall sutures are used [25, 27]. Suturing the electrodes arrays onto the wall will increase the contact with the tissue to give better recordings. However, sliding an elastic mesh over the heart to keep the electrodes in place is easier then suturing each electrode array in place [7].

Activation localization

Localizing the electrodes is a problem in most studies. As discussed earlier, using a regular pattern on a mesh for determining the positions of the electrodes is the easiest method. However, the location of activation will not correspond with the correct location that is indicated on the predetermined pattern. Using anatomical landmarks can improve the accuracy of locating the electrode position.

Other studies have used different solutions to localize the electrodes, such as MRI, CT, ultrasound, digitizer arm, and optical methods.
On a sock the electrodes are placed mostly in a regular pattern [2, 3, 4, 5, 6, 8, 10, 11, 14, 16, 19, 24, 28]. As the heart is contracting, the mesh will contract and expand with the movements of the heart, allowing the electrodes to remain in contact with the epicardium. This is not always possible as the shape of the heart is irregular, and during contraction some electrodes will lose contact. The pattern that is used to place the electrode on the heart is also used for displaying the activation patterns. A limitation of this method is that they assume that the inter electrode distance does not change when it is placed over the heart. However, it was noted that the inter electrode distance in fact changes as the mesh was stretched over the heart [27]. The actual recording locations will therefore be different from the estimated locations. When interpreting the results this will influence the representation of the activation patterns as the inter electrode distance is not constant. Furthermore, the heart is a beating organ, and with each contraction the distance between the electrodes will change, which results in a misrepresentation of the epicardial activation pattern depending the phase the heart is in.
To overcome the problem of changing inter electrode distance, flexible electrode arrays with a fixed inter electrode distance (Table 1) can be used [7,25, 27]. The electrode arrays are aligned on the epicardial surface using anatomical landmarks. With the fixed inter electrode distance, the electrode location of the whole array can be calculated on a 3D model if the position for a minimum of two electrodes is known [27]. Attaching the fixed arrays to the heart prevents the epicardial surface to slip from the electrode array. However, as was shown in [7], the area measured underneath the electrode array does not changes. This indicates that the fixed electrode array does not shift over the epicardial tissue. A limitation of using fixed electrode arrays, even though they are flexible and can conform to the shape of the heart, is that the heart has a complex shape and as it contracts, electrodes can dislodge from the surface and fail to record a signal. This can be prevented by suturing the array onto the epicardium or use a tight elastic mesh, however this might influence the epicardial conductivity which is undesirable.

Electrode locations are patient specific and need a custom heart model. In a generic heart model, the coordinate system of the digitizer arm does not match, making it difficult to align the data point. A custom model can be generated from only the electrode coordinates by interpolating between the points [24]. To improve the accuracy of the electrode locations on the heart, a digitizer arm can be used to locate the electrodes [13, 19, 24]. However, the accuracy of the 3D model is dependent on the number of data points, more data points result in a better model. To record all the electrode locations takes time, which is not always an option. A major limitation of using a digitizer arm is that access to the electrodes is required. For this reason, after *in vivo* experimentation the heart is excised. When doing a patient study, this is highly undesirable and should not be done.
To obtain a higher resolution model of the heart, ultrasound, MRI, or CT can be used [10, 16, 19]. The advantage of using ultrasound is that it can be easily applied, is an inexpensive technique, and can detect differences between tissue types. This also makes it possible to locate the electrodes on the heart. However, to make a 3D model of the images, the position of the transducer must be known making it more expensive [19]. When using MRI to create a 3D model, the materials must not affect the magnetic field, which may distort the image. In addition, metals are not visible on MRI images. A contrast agent is needed to localize the sock [10]. For this reason, material properties must be taken into account when designing an epicardial electrode array. When imaging the heart with MRI, the beating of the heart can cause motion artifacts. Motion artifacts can be reduced by cardiac gating, acquiring data at a specific point in the heart cycle over multiple beats. However, this makes it difficult to investigate the local epicardial activity of one heartbeat as the electrode location is acquired over multiple beats.
Using CT, the 3D model and electrode locations can be easily determined [16]. However, as with MRI, capturing images of the heart takes time, which can cause motion artifacts. This can also be reduced

by cardiac gating. Furthermore, CT and MRI are expensive imaging technologies. This makes it less ideal to use these techniques.
Finally, when obtaining the geometry of the heart optically, problems arise with the visibility of the heart. As the heart is a 3D shape, when recording images of the heart some parts of the heart shape will obstruct the view, this will reduce the accuracy of the model. Even when the heart is in a Langedorff setup, scanning and processing the surface of the heart takes time [13].This makes optical geometry reconstruction an uncommon method.

Conclusion

This literature review presents an overview of the techniques that are used for measuring epicardial activation patterns. Essential is locating the electrode positions on the epicardium. The best approach for recording the epicardial activation is by placing unipolar electrodes in an array. The electrode array should be fixed with an elastic sock to the heart. To visualize the epicardial activation pattern the shape of the sock can be used. However, localizing the electrodes on the sock remains a problem. Therefore, a novel method should be developed which can measure the inter electrode distance simultaneously with the epicardial recordings.

References

1. Amesz, J., Dekker, R., Taverne, Y. J. H. J., de Groot, N. M. S., Dankelman, J., & Knops, P. (2020). *Cardiac mapping on ex vivo perfused porcine slaughterhouse hearts: A Langendorff perfusion protocol for epicardial mapping on isolated beating hearts.* (Biomedical Engineering master thesis), Delft University of Technology. Retrieved from http://resolver.tudelft.nl/uuid:e2bc6f6b-ed3f-44b0-b851-74ea066a47c6
2. Arisi, G., Macchi, E., Baruffi, S., Spaggiari, S., & Taccardi, B. (1983). Potential fields on the ventricular surface of the exposed dog heart during normal excitation. *Circ Res, 52*(6), 706-715.
3. Bear, L. R., Walton, R. D., Abell, E., Coudière, Y., Haissaguerre, M., Bernus, O., & Dubois, R. (2019). Optical Imaging of Ventricular Action Potentials in a Torso Tank: A New Platform for Non-Invasive Electrocardiographic Imaging Validation. *Front Physiol, 10*, 146.
4. Brodine, W. N., Baker, K. A., Kirchmer, J. T., & Chiarelli, T. E. (1990). Simultaneous, multiple point mapping during surgery for Wolff-Parkinson-White syndrome without the use of a computer. *Pacing and clinical electrophysiology : PACE, 13*(9), 1096-1100.
5. Chattipakorn, N., KenKnight, B. H., Rogers, J. M., Walker, R. G., Walcott, G. P., Rollins, D. L., . . . Ideker, R. E. (1998). Locally propagated activation immediately after internal defibrillation. *Circulation, 97*(14), 1401-1410.
6. d'Alché, P., Clauser, P., Morel, M., & Gauthier, V. (1991). Assessment with potential mapping of the cardiac protective effect of a drug. Example of trimetazidine. *J Pharmacol Methods, 26*(1), 43-51.
7. Dhein, S., Müller, A., & Klaus, W. (1990). Nifedipine antagonizes ouabain-induced ST-segment changes and derangement of epicardial activation pattern in isolated rabbit hearts. *Int J Cardiol, 29*(2), 163-172.
8. Downar, E., Parson, I. D., Mickleborough, L. L., Cameron, D. A., Yao, L. C., & Waxman, M. B. (1984). On-line epicardial mapping of intraoperative ventricular arrhythmias: initial clinical experience. *J Am Coll Cardiol, 4*(4), 703-714.
9. Efimov, I. R., Fahy, G. J., Cheng, Y., Van Wagoner, D. R., Tchou, P. J., & Mazgalev, T. N. (1997). High-resolution fluorescent imaging does not reveal a distinct atrioventricular nodal anterior input channel (fast pathway) in the rabbit heart during sinus rhythm. *J Cardiovasc Electrophysiol, 8*(3), 295-306.
10. Faris, O. P., Evans, F. J., Ennis, D. B., Helm, P. A., Taylor, J. L., Chesnick, A. S., Guttman, M., a., Ozturk, C., McVeigh, E. R. (2003). Novel technique for cardiac electromechanical mapping

with magnetic resonance imaging tagging and an epicardial electrode sock. *Ann Biomed Eng, 31*(4), 430-440.
11. Harrison, L., Ideker, R. E., Smith, W. M., Klein, G. J., Kasell, J., Wallace, A. G., & Gallagher, J. J. (1980). The sock electrode array: a tool for determining global epicardial activation during unstable arrhythmias. *Pacing and clinical electrophysiology : PACE, 3*(5), 531-540.
12. Kappler, B., Ledezma, C. A., van Tuijl, S., Meijborg, V., Boukens, B. J., Ergin, B., . . . de Mol, B. A. J. M. (2019). Investigating the physiology of normothermic *ex vivo* heart perfusion in an isolated slaughterhouse porcine model used for device testing and training. *BMC Cardiovascular Disorders, 19*(1), 254. doi:10.1186/s12872-019-1242-9
13. Kay, M. W., Amison, P. M., & Rogers, J. M. (2004). Three-dimensional surface reconstruction and panoramic optical mapping of large hearts. *IEEE Transactions on Biomedical Engineering, 51*(7), 1219-1229. doi:10.1109/tbme.2004.827261
14. Kubota, I., Yamaki, M., Shibata, T., Ikeno, E., Hosoya, Y., & Tomoike, H. (1993). Role of ATP-sensitive K+ channel on ECG ST segment elevation during a bout of myocardial ischemia. A study on epicardial mapping in dogs. *Circulation, 88*(4 Pt 1), 1845-1851.
15. Lavier, S., Meunier, J., & Savard, P. (1993, 5-8 Sept. 1993). *Dynamic electrophysiological data visualization on a 3D model of the human heart.* Paper presented at the Proceedings of Computers in Cardiology Conference.
16. Massé, S., Sevaptsidis, E., Parson, I. D., & Downar, E. (1991). A three-dimensional display for cardiac activation mapping. *Pacing and clinical electrophysiology : PACE, 14*(4 Pt 1), 538-545.
17. Milani-Nejad, N., & Janssen, P. M. L. (2014). Small and large animal models in cardiac contraction research: advantages and disadvantages. *Pharmacology & therapeutics, 141*(3), 235-249. doi:10.1016/j.pharmthera.2013.10.007
18. Mouws, E., Lanters, E. A. H., Teuwen, C. P., van der Does, L., Kik, C., Knops, P., . . . de Groot, N. M. S. (2018). Impact of Ischemic and Valvular Heart Disease on Atrial Excitation:A High-Resolution Epicardial Mapping Study. *J Am Heart Assoc, 7*(6).
19. Nash, M. P., Bradley, C. P., Kardos, A., Pullan, A. J., & Paterson, D. J. (2002). An experimental model to correlate simultaneous body surface and epicardial electropotential recordings in vivo. *Chaos, Solitons & Fractals, 13*(8), 1735-1742. doi:https://doi.org/10.1016/S0960-0779(01)00165-5
20. Qu, F., Ripplinger, C. M., Nikolski, V. P., Grimm, C., & Efimov, I. R. (2007). Three-dimensional panoramic imaging of cardiac arrhythmias in rabbit heart. *J Biomed Opt, 12*(4), 044019.
21. Raftis, J. B., Mills, N. L., & Duffin, R. (2017). Chapter 11 - Cardiovascular System. In B. Fadeel, A. Pietroiusti, & A. A. Shvedova (Eds.), *Adverse Effects of Engineered Nanomaterials (Second Edition)* (pp. 255-274): Academic Press.
22. Rodriguez, B., Trayanova, N., & Noble, D. (2006). Modeling cardiac ischemia. *Ann N Y Acad Sci, 1080*, 395-414. doi: 10.1196/annals.1380.029
23. Swift, L. M., Jaimes, R., 3rd, McCullough, D., Burke, M., Reilly, M., Maeda, T., . . . Posnack, N. G. (2019). Optocardiography and Electrophysiology Studies of *Ex Vivo* Langendorff-perfused Hearts. *Journal of visualized experiments : JoVE*(153), 10.3791/60472. doi:10.3791/60472
24. Taccardi, B., Lux, R. L., Ershler, P. R., MacLeod, R. S., Zabawa, C., & Vyhmeister, Y. (1992, 11-14 Oct. 1992). *Potential distributions and excitation time maps recorded with high spatial resolution from the entire ventricular surface of exposed dog hearts.* Paper presented at the Proceedings Computers in Cardiology.
25. Wang, Y., Yang, C., & Yu, J. (2014, 14-16 Oct. 2014). *Implementation of real-time isopotential map in epicardial mapping system.* Paper presented at the 2014 7th International Conference on Biomedical Engineering and Informatics.
26. Wijns, W., Crea, F., & Lanza, G. A. (2020). ESC CardioMed *Myocardial ischaemia: definition and causes*: Oxford University Press.
27. Wit, A. L., Allessie, M. A., Bonke, F. I., Lammers, W., Smeets, J., & Fenoglio, J. J., Jr. (1982). Electrophysiologic mapping to determine the mechanism of experimental ventricular

tachycardia initiated by premature impulses. Experimental approach and initial results demonstrating reentrant excitation. *Am J Cardiol, 49*(1), 166-185.
28. Worley, S. J., Ideker, R. E., Mastrototaro, J., Smith, W. M., Vidaillet, H., Jr., Chen, P. S., & Lowe, J. E. (1987). A new sock electrode for recording epicardial activation from the human heart: one size fits all. *Pacing and clinical electrophysiology : PACE, 10*(1 Pt 1), 21-31.
29. Yaksh, A., Kik, C., Knops, P., Roos-Hesselink, J. W., Bogers, A. J., Zijlstra, F., . . . de Groot, N. M. (2014). Atrial fibrillation: to map or not to map? *Neth Heart J, 22*(6), 259-266.
30. Yaksh, A., van der Does, L. J. M. E., Kik, C., Knops, P., Oei, F. B. S., van de Woestijne, P. C., . . . de Groot, N. M. S. (2015). A novel intra-operative, high-resolution atrial mapping approach. *Journal of interventional cardiac electrophysiology : an international journal of arrhythmias and pacing, 44*(3), 221-225. doi:10.1007/s10840-015-0061-x
31. Zenger, B., Good, W. W., Bergquist, J. A., Rupp, L. C., Perez, M., Stoddard, G. J., . . . MacLeod, R. S. (2021). Pharmacological and simulated exercise cardiac stress tests produce different ischemic signatures in high-resolution experimental mapping studies. *J Electrocardiol, 68*, 56-64.

Appendix D Background information

1.1 The heart

The heart is the most important muscle in the circulatory system and its primary function is to pump blood through our body. The heart muscle is made up of three layers, the epicardium, myocardium, and endocardium. The epicardium is the superficial layer of the heart. It is the visceral layer of the serous pericardium, a fibrous serous membrane that forms a sac around the heart, and allows the heart to slide with almost no friction in the pericardial sock [1]. The middle layer of the heart wall is the myocardium. It mainly consists of cardiac muscle cells and connective tissue. The cardiac muscle cells form branching fibers and are the reason the heart can contract. The connective tissue gives the heart its structure and holds all the different parts together [1]. The last layer is the endocardium, which lines the four chambers of the heart. It makes the wall a smooth surface and plays a role in blood clotting, inflammation, blood fluidity, angiogenesis, and vascular tone [2].

The heart has four chambers through which the blood flows (see figure 1). It receives blood in the atria and pumps the blood to the ventricles. Low O_2 and carbon dioxide (CO_2) rich blood enters the right atrium and is pumped into the pulmonary arteries from the right ventricles. The pulmonary arteries carry the blood to the lungs, where it expels CO_2 from the blood and takes O_2 up in the blood. The O_2 rich blood enters the heart from the left atrium and is pumped into the systemic circuit by the left ventricle. Valves located between the four chambers prevent blood from flowing backward.

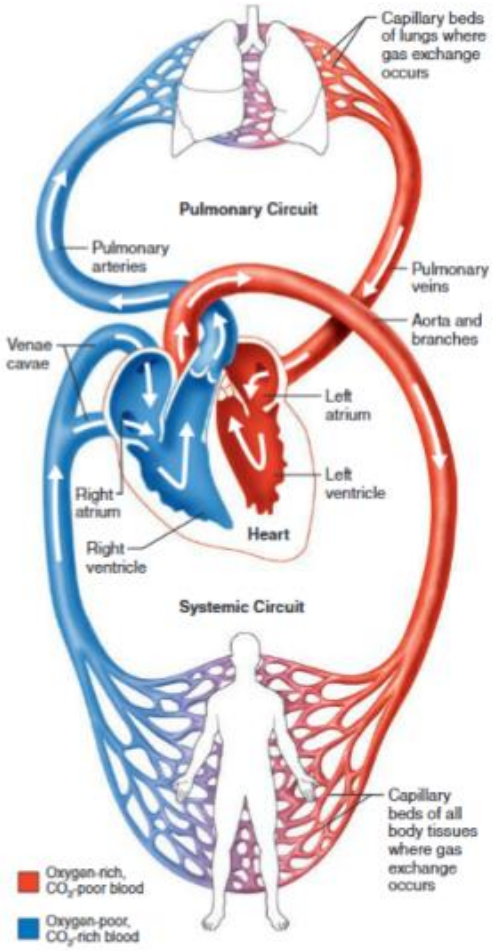

Figure 6 The circulatory system and the path the blood flows through the human body. Image taken from [1]

1.2. Electrophysiology

The muscle fibers of the heart are activated by an electrical pulse generated by the sinoatrial (SA) node, located in the right atrium in the sulcus terminalis near the vena cava superior[3]. As the muscle fibers are activated by the electrical signal, the fibers of the heart will contract. The contraction of the heart will cause an increase in the pressure of the chambers and the blood is pushed into the blood vessels. The sequence of activation of the heart fibers plays an important role in the function of the heart. An abnormality in the activation sequence can cause health problems, and in extreme cases, even death. The cells in the SA node are pacemakers cells. Ions will slowly leak out of the cell, causing a decrease in the voltage difference over the cell membrane. If the voltage difference reaches a certain threshold, the cells will generate an impulse and start the contraction of the heart. During normal heart rhythm, electrical activation starts at the SA node (see figure 2)[3]. The pulse propagates from the SA node over the left and right atrium where it will finally reach the atrioventricular (AV) node, located in the Koch triangle near the coronary sinus on the interatrial septum[3,4]. In the AV node, the signal propagation has a small delay before it travels to the ventricles. During this time, the atria contract and the ventricles are filled with blood.
After the small delay, the electrical signal travels through the His bundle where it splits into the Purkinje fibers. From the Purkinje fibers, the electrical signal is guided to the apex of the heart. At the apex, the signal turns superiorly into the ventricular walls to the atrioventricular groove. Contraction of the heart follows the activation patterns of the heart and starts at the apex and follows the electrical activation to the top of the ventricles where it butts up against the atria[1].

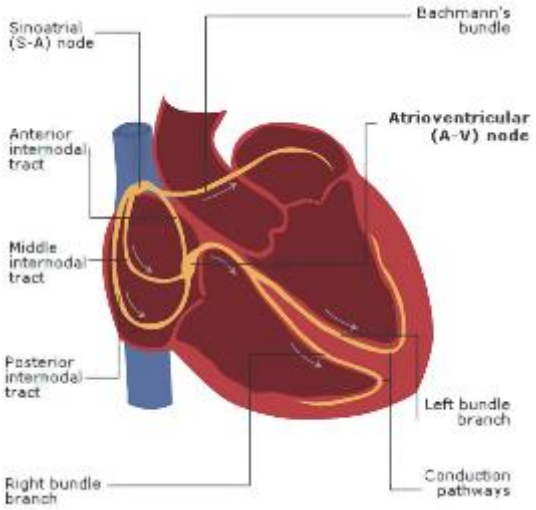

Figure 7. The anatomy of the conductive system of the heart. Image taken from [1].

References

1. Marieb, E.N. and K. Hoehn, *Human anatomy & physiology*. 2016, Pearson Education Limited: Harlow.
2. Félétou, M., 2011.
7. Macfarlane, P.W., *Comprehensive electrocardiology*. 2011, Springer: New York ;.
8. Heaton, J. and A. Goyal, *Atrioventricular Node.* 2022.